

Computing Extremal Teichmüller Map of Multiply-Connected Domains Via Beltrami Holomorphic Flow

Tsz Ching Ng · Xianfeng Gu · Lok Ming Lui

Received: 22 March 2013 / Revised: 27 August 2013 / Accepted: 8 October 2013 /
Published online: 20 October 2013
© Springer Science+Business Media New York 2013

Abstract A numerical method for computing the extremal Teichmüller map between multiply-connected domains is presented. Given two multiply-connected domains, there exists a unique Teichmüller map (T-Map) between them minimizing the conformality distortion. The extremal T-Map can be considered as the ‘most conformal’ map between multiply-connected domains. In this paper, we propose an iterative algorithm to compute the extremal T-Map using the Beltrami holomorphic flow (BHF). The BHF procedure iteratively adjusts the initial map based on a sequence of Beltrami coefficients, which are complex-valued functions defined on the source domain. It produces a sequence of quasi-conformal maps, which converges to the T-Map minimizing the conformality distortion. We test our method on synthetic data together with real human face data. Results show that our algorithm computes the extremal T-Map between two multiply-connected domains of the same topology accurately and efficiently.

Keywords Teichmüller map · Extremal map · Multiply-connected · Beltrami holomorphic flow · Beltrami coefficient · Quasiconformal map

1 Introduction

Establishing meaningful mappings between different domains is an important research topic in many fields. Applications can be found in different areas such as registration, shape analysis and grid generation. Conformal mapping has been widely used to establish a good one-to-one correspondence between different domains, since it preserves the local geometry well

T. C. Ng · L. M. Lui (✉)
Department of Mathematics, The Chinese University of Hong Kong,
Shatin, New Territories, Hong Kong
e-mail: lmlui@math.cuhk.edu.hk

X. Gu
Department of Computer Science, State University of New York at Stony Brook,
Stony Brook, NY, USA

[3,4,8–12,24,27]. According to the Riemann mapping theorem, conformal mappings between simply-connected domains always exist. However, this fact is not valid for multiply-connected domains. Given two multiply-connected domains with different conformal modules, there is generally no conformal mapping between them. In this case, it is usually desirable to obtain a mapping that minimizes the conformality distortion. Every diffeomorphic mapping is associated with a unique Beltrami coefficient (BC), which is a complex-valued function, μ_f , defined on the source domain. The BC, μ_f , measures the deviation of the mapping from a conformal map. Given two multiply-connected domains Ω_1 and Ω_2 , there exists a unique and bijective map $f : \Omega_1 \rightarrow \Omega_2$, called the *extremal Teichmüller map* (T-Map), minimizing the L^∞ norm of the BC [5]. Therefore, the extremal T-Map can be considered as the ‘most conformal’ map between multiply-connected domains, which is a natural extension of conformal mappings.

In this work, our goal is to numerically compute the extremal T-Map between two multiply-connected domains Ω_1 and Ω_2 of the same topology. Mathematically, we want to solve the following:

$$f^* = \operatorname{argmin}_{f:\Omega_1 \rightarrow \Omega_2} \{ \|\mu_f\|_\infty \} \quad (1)$$

such that f^* is a diffeomorphism between Ω_1 and Ω_2 .

We present in this paper a numerical method to solve the above optimization problem. The domains of interest can either be planar domains or surfaces embedded in \mathbb{R}^3 . We propose an iterative algorithm to obtain the extremal T-Map using the Beltrami holomorphic flow (BHF). The BHF procedure iteratively adjusts the initial map, based on a sequence of Beltrami coefficients. It produces a sequence of quasi-conformal maps, which converges to the desired extremal T-Map. Numerical experiments have been carried out on synthetic data together with real human face data. Numerical results show that our algorithm computes the extremal T-Map between multiply-connected domains accurately and efficiently.

The rest of the paper is organized as follows. In Sect. 2, we review some previous works closely related to this paper. In Sect. 3, we describe some basic mathematical background necessary for explaining this work. In Sect. 4, we formulate the mathematical problem in details. Our proposed algorithm to compute the extremal T-Map is discussed in Sect. 5. The detailed numerical implementation of our proposed model is explained in Sect. 6. In Sect. 7, we show the numerical results to demonstrate the effectiveness of the proposed method. A concluding remark and a discussion of future directions are given in Sect. 8.

2 Related Work

Extremal T-Maps are closely related to conformal mappings. Simply-speaking, an extremal T-Map is the optimal quasi-conformal map that is closest to conformal. The computation of conformal mappings have been extensively studied [3,4,8–12,24,27]. For example, Hurdal et al. [12] proposed to compute the conformal parameterizations using circle packing and applied it to register human brains. Porter [24] proposed to use the interpolating polynomial method for computing the conformal mappings of simply-connected planar domains. Gu et al. [8,9,27] proposed to compute the conformal parameterizations of Riemann surfaces for the purpose of registration using harmonic energy minimization and holomorphic 1-forms. Later, the authors proposed the curvature flow method to compute conformal parameterizations of high-genus surfaces onto their universal covering spaces [13,30,32]. Hale et al. [11] proposed to compute conformal maps to multiply-slit domains by using a Schwarz–Christoffel formulation. DeLillo et al. [3] proposed a numerical method to compute the

Schwarz–Christoffel transformation for multiply-connected domains. Conformal maps have been widely used since it preserves the local geometry well.

In real world situations, mappings are usually quasi-conformal (QC), which induce bounded amount of conformality distortion. The numerical computation of quasi-conformal maps have been widely studied. Mastin et al. [22] proposed to use finite difference methods to compute QC mappings on complex plane. These methods are difficult to implement for arbitrary regions. Later, the authors proposed a finite difference scheme for constructing QC mappings for arbitrary simply and doubly-connected region of the plane onto a rectangle [23]. In [1], Daripa proposed a numerical construction of QC mappings in the plane by solving the Beltrami equation. This method was further extended to compute the QC map of an arbitrary doubly connected domain with smooth boundaries onto an annulus [2]. All of these methods deal with simple domains in the complex plane. Recently, surface QC maps have also been studied. Lui et al. [20] proposed to compute quasi-conformal registration between hippocampal surfaces which matches geometric quantities (such as curvatures) as much as possible. A method called the Beltrami holomorphic flow is used to obtain the optimal Beltrami coefficient associated to the registration [17, 19, 21, 29]. Beltrami coefficient has been applied to represent general surface homeomorphisms, which is comparatively easier to manipulate than 3D coordinate functions. Using the Beltrami representation, compression of surface maps has been proposed [19], which can be applied for video compression [17]. Wei et al. [31] also proposed to compute QC mapping for feature matching face registration. The Beltrami coefficient associated to a landmark points matching parameterization is approximated. However, either exact landmark matching or the bijectivity of the mapping cannot be guaranteed, especially when very large deformations occur. In order to compute QC mapping from the Beltrami coefficients effectively, Quasi-Yamabe method was introduced, which applied the curvature flow method to compute the QC mapping [33]. The algorithm can deal with surfaces with general topologies. Later, extremal QC mappings, which minimize conformality distortion has been proposed. Zorin et al. [28] proposes a least square algorithm to compute mapping between connected domains with given Dirichlet condition defined on the whole boundaries. The extremal mapping is obtained by minimizing a least square Beltrami energy, which is non-convex. The algorithm can obtain an extremal mapping when initialization is carefully chosen. However, the convergence to the global minimum and the bijectivity of the mapping cannot be guaranteed. Recently, Lui et al. [18] proposed to compute the unique T-Map between simply-connected Riemann surfaces of finite type. The proposed algorithm was applied for landmark-based surface registration.

3 Overview of Quasi-Conformal Geometry

In this section, we describe some basic mathematical concepts relevant to our algorithms. For details, we refer the readers to [6, 14].

A surface S with a conformal structure is called a *Riemann surface*. Given two Riemann surfaces M and N , a map $f : M \rightarrow N$ is *conformal* if it preserves the surface metric up to a multiplicative factor called the *conformal factor*. A generalization of conformal maps is the *quasi-conformal* maps, which are orientation preserving homeomorphisms between Riemann surfaces with bounded conformality distortion, in the sense that their first order approximations takes small circles to small ellipses of bounded eccentricity [6]. Mathematically, $f : \mathbb{C} \rightarrow \mathbb{C}$ is quasi-conformal provided that it satisfies the Beltrami equation:

$$\frac{\partial f}{\partial \bar{z}} = \mu(z) \frac{\partial f}{\partial z}. \quad (2)$$

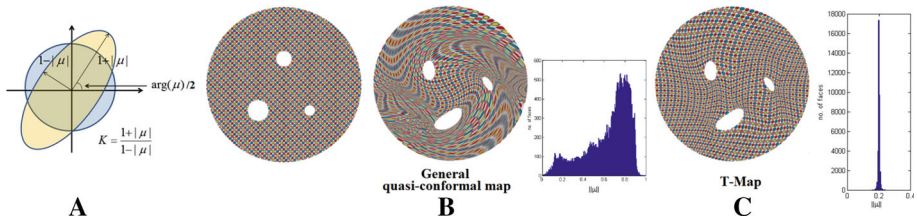


Fig. 1 **a** Illustrates how the conformality distortion under a quasi-conformal map can be determined by μ . **b** A general quasi-conformal map visualized by texture mapping. It illustrates that conformality distortion is not necessarily uniform for a general quasi-conformal map. **c** A Teichmüller map, whose conformality distortion is uniform everywhere. The histograms in **(b)**, **(c)** the distributions of the norms of the associated Beltrami coefficients. Sparsity of the histogram measures the uniformity of the conformality distortion

for some complex-valued function μ satisfying $\|\mu\|_\infty < 1$. μ is called the *Beltrami coefficient*, which is a measure of non-conformality. μ_f measures how far the map is deviated from a conformal map. $\mu \equiv 0$ if and only if f is conformal. Infinitesimally, around a point p , f may be expressed with respect to its local parameter as follows:

$$\begin{aligned} f(z) &= f(p) + f_z(p)z + f_{\bar{z}}(p)\bar{z} \\ &= f(p) + f_z(p)(z + \mu(p)\bar{z}). \end{aligned} \tag{3}$$

Obviously, f is not conformal if and only if $\mu(p) \neq 0$. Inside the local parameter domain, f may be considered as a map composed of a translation to $f(p)$ together with a stretch map $S(z) = z + \mu(p)\bar{z}$, which is postcomposed by a multiplication of $f_z(p)$. All the conformal distortion of $S(z)$ is caused by $\mu(p)$. $S(z)$ is the map that causes f to map a small circle to a small ellipse. From $\mu(p)$, we can determine the directions of maximal magnification and shrinking and the amount of their distortions as well. Specifically, the angle of maximal magnification is $\arg(\mu(p))/2$ with magnifying factor $1 + |\mu(p)|$; The angle of maximal shrinking is the orthogonal angle $(\arg(\mu(p)) - \pi)/2$ with shrinking factor $1 - |\mu(p)|$. Thus, the Beltrami coefficient μ gives us all the information about the properties of the map (see Fig. 1a).

The maximal dilation of f is given by:

$$K(f) = \frac{1 + \|\mu\|_\infty}{1 - \|\mu\|_\infty}. \tag{4}$$

Quasiconformal mapping between two Riemann surfaces R_1 and R_2 can also be defined. Instead of the Beltrami coefficient, the *Beltrami differential* has to be used. A Beltrami differential $\mu(z) \frac{d\bar{z}}{dz}$ on the Riemann surface R_1 is an assignment to each chart (U_α, ϕ_α) of an L^∞ complex-valued function μ_α , defined on local parameter z_α such that

$$\mu_\alpha(z_\alpha) \frac{d\bar{z}_\alpha}{dz_\alpha} = \mu_\beta(z_\beta) \frac{d\bar{z}_\beta}{dz_\beta}, \tag{5}$$

on the domain which is also covered by another chart (U_β, ϕ_β) , where $\frac{dz_\beta}{dz_\alpha} = \frac{d}{dz_\alpha} \phi_{\alpha\beta}$ and $\phi_{\alpha\beta} = \phi_\beta \circ \phi_\alpha^{-1}$.

An orientation preserving diffeomorphism $f : R_1 \rightarrow R_2$ is called quasi-conformal associated with $\mu(z) \frac{d\bar{z}}{dz}$ if for any chart (U_α, ϕ_α) on R_1 and any chart (V_β, ψ_β) on R_2 , the mapping $f_{\alpha\beta} := \psi_\beta \circ f \circ \phi_\alpha^{-1}$ is quasi-conformal associated with $\mu_\alpha(z_\alpha) \frac{d\bar{z}_\alpha}{dz_\alpha}$.

4 The Mathematical Formulation of the Problem

4.1 The Extremal Problem

Given two multiply-connected domains or surfaces Ω_1 and Ω_2 , both with $n + 1$ boundaries. Denote the boundaries of Ω_1 and Ω_2 by $\{\gamma_0, \gamma_1, \dots, \gamma_n\}$ and $\{\gamma'_0, \gamma'_1, \dots, \gamma'_n\}$ respectively. Conformal maps between arbitrary multiply-connected domains generally do not exist. One might be interested in studying extremal quasi-conformal mappings, which are extremal in the sense of minimizing the $\|\cdot\|_\infty$ over all Beltrami differentials corresponding to quasi-conformal mappings between Ω_1 and Ω_2 . The idea of extremality is to make $K(f)$ as small as possible such that f is as ‘nearly conformal’ as possible. Extremal mapping always exists but needs not to be unique.

Let $f : \Omega_1 \rightarrow \Omega_2$ be a quasi-conformal mapping between Ω_1 and Ω_2 . Assume that f satisfies the boundary condition: $f(\gamma_i) = \gamma'_i$ for all i . Note that the point-wise correspondences between the boundaries are not required. f is said to be an *extremal mapping* if for any quasi-conformal mapping $h : \Omega_1 \rightarrow \Omega_2$ satisfying the boundary condition,

$$K(f) \leq K(h) \tag{6}$$

It is called *uniquely extremal* if the inequality (6) is strict for $h \neq f$ [25,26].

Note that an extremal mapping is not unique for general cases. According to Eq. (4), $K(f)$ is minimum if and only if $\|\mu(f)\|_\infty$ is minimized. The extremal problem can therefore be expressed as finding $f^* : \Omega_1 \rightarrow \Omega_2$ that solves:

$$f^* = \mathbf{argmin}_{f \in \mathcal{A}} \{\|\mu_f\|_\infty\} \tag{7}$$

where $\mathcal{A} = \{f : \Omega_1 \rightarrow \Omega_2 : f \text{ is a quasi-conformal map, } f(\gamma_i) = \gamma'_i \text{ for } 0 \leq i \leq n\}$.

The extremal map is closely related to another type of mapping, called the *Teichmüller map* (*T-Map*). Simply-speaking, a T-Map is a quasi-conformal map with uniform conformality distortion. Mathematically, a quasi-conformal map g is said to be a T-Map associated with an integrable holomorphic function $\varphi : \Omega_1 \rightarrow \mathbb{C}$ if its associated Beltrami coefficient is of the form:

$$\mu(g) = k \frac{\bar{\varphi}}{|\varphi|} \tag{8}$$

for some constant $0 \leq k < 1$ and integrable holomorphic function $\varphi \neq 0$. The Beltrami coefficient of this form is said to be of *Teichmüller type*.

Figure 1b, c shows the difference between a general quasi-conformal map and a T-Map. (b) shows a general quasi-conformal map visualized by texture mapping. The small circles on the source domain are mapped to small ellipses on the target domain with different eccentricity (see the histogram of the norm of its Beltrami coefficient). (c) shows a T-Map visualized by texture mapping. The small circles on the source domain are mapped to small ellipses on the target domain with uniform eccentricity everywhere. As we can see from the histogram, the norm of the Beltrami coefficient accumulates at 0.3.

In general, there are many T-maps between two multiply-connected domains with the same topology. In particular, given the boundary correspondence $h : \partial\Omega_1 \rightarrow \partial\Omega_2$ satisfying $h'(e^{i\theta}) \neq 0$ and $|h''(e^{i\theta})| < \infty$, there exists a unique T-Map between Ω_1 and Ω_2 [25]. An important observation is that the T-Map is uniquely extremal for its boundary values.

Theorem 1 *Let Ω_1 and Ω_2 be multiply-connected domains with the same topology and $h : \partial\Omega_1 \rightarrow \partial\Omega_2$. Suppose $f : \Omega_1 \rightarrow \Omega_2$ is a Teichmüller map with a quadratic differential of finite norm, with $f|_{\partial\Omega_1} = h$. Then f is uniquely extremal for its boundary values.*

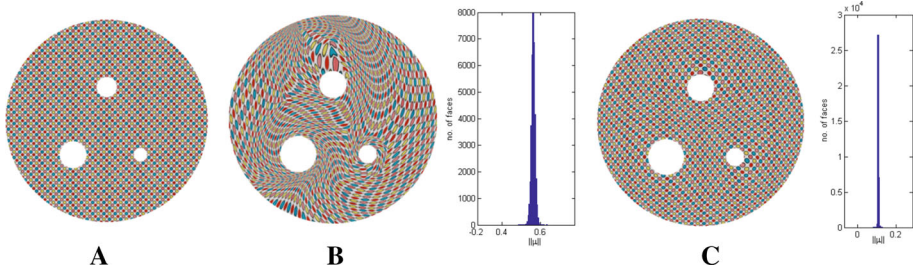


Fig. 2 T-Maps with different maximal dilations. **a, b** Two circle domains with three holes. **b** A T-Map, visualized by texture mapping. Its BC norm is equal to 0.58. **c** The extremal T-Map, whose BC norm (=0.11) is minimum over all possible T-Maps

Proof Suppose g is an extremal extension of h . Let the Beltrami coefficient of f be $\mu_f = k \frac{\bar{\varphi}}{\varphi}$. Since f and g agrees on their boundaries, the following inequality holds [25]:

$$\int_{\Omega_1} \frac{(|\alpha|^2 - |\beta|^2) + (1 - |\mu_f|)(|\alpha| - \mathbf{Re}(\frac{\bar{\beta}\alpha}{|\alpha|}))}{(1 + |\mu_f|)(1 - |\beta|^2)} |\varphi| \leq \mathbf{Re} \int_{\Omega_1} \frac{\bar{\alpha}}{\alpha} \left(|\varphi| - \frac{\mu_f}{|\mu_f|} \varphi \right) \frac{(1 - \bar{\beta}\alpha)(\alpha - \beta)}{(1 - |\mu_f|^2)(1 - |\beta|^2)} \tag{9}$$

where $\alpha = \mu_{f^{-1}} \circ f$; $\beta = \mu_{g^{-1}} \circ g$. Since $\mu_f = k \frac{\bar{\varphi}}{\varphi}$, the right-hand side of (9) vanishes. Hence, $\alpha = \beta$. This implies: $\mu_{f^{-1}} = \mu_{g^{-1}}$. Since f^{-1} and g^{-1} has the same boundary values, namely, h^{-1} , we have $f^{-1} = g^{-1}$. Thus, f is the unique extremal map satisfying the boundary values h . \square

Therefore, with different boundary value $h : \partial\Omega_1 \rightarrow \partial\Omega_2$, different T-Map can be obtained (see Fig. 2). We denote the collection of all possible Beltrami coefficients of Teichmüller type associated with quasi-conformal maps between Ω_1 and Ω_2 by $\mathfrak{T}(\Omega_1, \Omega_2)$. In other words,

$$\mathfrak{T}(\Omega_1, \Omega_2) := \left\{ v = k \frac{\bar{\varphi}}{|\varphi|} \mid 0 \leq k < 1, \varphi \text{ integrable holomorphic, } v = \mu(f) \text{ for some } f : \Omega_1 \rightarrow \Omega_2 \right\}. \tag{10}$$

Our goal is to look for the optimal $v^* := k^* \frac{\bar{\varphi}^*}{|\varphi^*|} \in \mathfrak{T}(\Omega_1, \Omega_2)$ whose $\|v^*\|_\infty (= k^*)$ is minimized over $\mathfrak{T}(\Omega_1, \Omega_2)$. It turns out that v^* is the unique minimizer. It is also the Beltrami coefficient associated with the unique extremal map between Ω_1 and Ω_2 (see Fig. 2). This is guaranteed by the following theorem.

Theorem 2 *Let Ω_1 and Ω_2 be multiply-connected domains with the same topology but with different conformal modules. Assume that Ω_1 has no conformal self-mapping. Then, there exists a unique extremal map $f : \Omega_1 \rightarrow \Omega_2$ satisfying the boundary condition: $f(\gamma_i) = \gamma'_i$ for all i . Also, f is a T-Map associated with an integrable holomorphic quadratic function on Ω_1 .*

Proof By the compactness argument, there exists an extremal map $f_{ext} : \Omega_1 \rightarrow \Omega_2$ with $f_{ext}(\gamma_i) = \gamma'_i$ for all i such that $\|\mu(f_{ext})\|_\infty = \inf_{f: \Omega_1 \rightarrow \Omega_2} \{\|\mu(f)\|_\infty\} := k$. Let $h = f_{ext}|_{\partial\Omega_1}$. We proceed to prove that f_{ext} is unique and is a Teichmüller map.

By Theorem 1, there exists a unique Teichmüller map $f : \Omega_1 \rightarrow \Omega_2$ such that $f|_{\partial\Omega_1} = h$. f is the unique extremal map for the boundary value h . Hence, $f_{ext} = f$. Hence, all extremal map between Ω_1 and Ω_2 must be a Teichmüller map.

Now, suppose $g : \Omega_1 \rightarrow \Omega_2$ is another extremal map. Since $g^{-1} \circ f$ is homotopic to identity, we conclude that either there exists a set of positive measure on Ω_1 for which $|\mu(g)(z)| > k$ or $\mu(g) = \mu(f)$ [5]. Since g is extremal, $\|\mu(g)\|_\infty = k$. Hence, $\mu(g) = \mu(f)$ is of Teichmüller type. This implies $g^{-1} \circ f$ is conformal and thus $f = g$. \square

Theorems 1 and 2 play the fundamental roles in this paper for us to develop the iterative algorithm to compute the extremal T-Map.

4.2 Variational Formulation of the Extremal Problem

In this section, we give a variational formulation of the extremal problem. The T-Map can then be computed through optimization techniques.

Recall that an extremal T-Map is extremal in the sense of minimizing the $\|\cdot\|_\infty$ over all Beltrami differentials. According to Theorem 2, the unique extremal map between multiply-connected domains is a T-Map. Therefore, our goal is to look for a T-Map minimizing the conformality distortion. The extremal problem can then be formulated as follows:

$$f^* = \mathbf{argmin}_{f:\Omega_1 \rightarrow \Omega_2} E_1(f) = \mathbf{argmin}_{f:\Omega_1 \rightarrow \Omega_2} \{\|\mu(f)\|_\infty\} \tag{11}$$

subject to:

- $f^*(\gamma_i) = \gamma'_i$ for $i = 0, 1, 2, \dots, n$ (boundary condition);
- $\mu(f^*) = k \frac{\bar{\varphi}}{\varphi}$ for some constant $0 \leq k < 1$ and integrable holomorphic function $\varphi : \Omega_1 \rightarrow \mathbb{C}$ ($\varphi \neq 0$).

However, minimizing $E_1(f)$ with respect to the space of quasi-conformal maps between Ω_1 and Ω_2 is difficult. In fact, let $f = f_1 + if_2$, the minimization problem can be expanded as follows:

$$f^* = \mathbf{argmin}_f \{\|\mu(f)\|_\infty\} = \mathbf{argmin}_f \left\{ \left\| \frac{\partial f / \partial \bar{z}}{\partial f / \partial z} \right\|_\infty \right\} \tag{12}$$

subject to $f^*(\gamma_i) = \gamma'_i$ ($i = 0, 1, 2, \dots, n$) and $\mu(f^*) = k \frac{\bar{\varphi}}{\varphi}$ for some constant $0 \leq k < 1$ and integrable holomorphic function $\varphi : \Omega_1 \rightarrow \mathbb{C}$ ($\varphi \neq 0$).

In order to minimize the above constrained minimization problem effectively, we propose to reformulate the above problem to an optimization problem over the space of all Beltrami coefficients:

$$(v^*, f^*) = \mathbf{argmin}_{v:\Omega_1 \rightarrow \mathbb{C}} E_2(v) := \mathbf{argmin}_{v:\Omega_1 \rightarrow \mathbb{C}} \{\|v\|_\infty\} \tag{13}$$

subject to:

- $v^* = \mu(f^*)$ and $\|v^*\|_\infty < 1$;
- $v^* = k \frac{\bar{\varphi}}{\varphi}$ for some constant $0 \leq k < 1$ and holomorphic function $\varphi : \Omega_1 \rightarrow \mathbb{C}$;
- $f^*(\gamma_i) = \gamma'_i$ for $i = 0, 1, 2, \dots, n$ (boundary condition).

Minimizing E_2 with respect to BCs subject to the constraints is advantageous since the diffeomorphic property of the mapping can be easily controlled. Every diffeomorphism is associated with a smooth Beltrami coefficient $\mu(f)$. $\mu(f)$ measures the bijectivity (1-1 and onto) of f . In fact, $\mu(f)$ is related to the Jacobian $J(f)$ of f by the following formula:

$$J(f) = \left| \frac{\partial f}{\partial z} \right|^2 (1 - |\mu(f)|^2) \tag{14}$$

Therefore, the map f is bijective if $|\mu(f)|$ is everywhere less than 1. When solving the minimization problem (13), the bijectivity of the mapping in each iteration can be ensured by enforcing $\|v\|_\infty < 1$. Our goal is to look for a sequence of $\{v_n\}_{n=1}^\infty$ converging to the optimal BC, v^* , which corresponds to our desired extremal T-Map, f^* . Another advantage of the reformulation is that we can alternatively minimize (13) with respect to v and minimize $\|v - \mu(f)\|_\infty$ with respect to f in the implementation.

In Sect. 5, we describe a numerical algorithm to obtain such a sequence.

5 Proposed Algorithm

We describe our proposed method to compute the T-Map in this section.

5.1 Beltrami Holomorphic Flow (BHF)

Finding the extremal T-Map is equivalent to finding its associated Beltrami coefficient(BC). As BC varies, its associated quasi-conformal map varies and vice versa. We first examine the relationship between the variation of BCs and their associated quasi-conformal maps.

Let $f^\mu : \Omega_1 \rightarrow \Omega_2$ be a quasi-conformal map, whose BC is $\mu : \Omega_1 \rightarrow \mathbb{C}$. Assume μ varies by ω , and assume its associated quasiconformal map $f^{\mu+\omega}$ varies by \mathbf{V} . In other words, $f^{\mu+\omega}(z) = f^\mu(z) + \mathbf{V}(z)$. Obviously, \mathbf{V} depends on v . In fact, if $f^{\mu+t\omega}(z) = f^\mu(z) + \mathbf{V}_t(z)$ ($t \in \mathbb{C}$), then $\mathbf{V}_t(z)$ depends holomorphically on $t \in \mathbb{C}$ [6]. We call the flow from f^μ to $f^{\mu+t\omega} = f^\mu(z) + \mathbf{V}_t(z)$ the *Beltrami holomorphic flow* (BHF) from μ to $\mu + t\omega$ [17, 19, 21, 29]. In particular, $\mathbf{V}(z) = \mathbf{V}_1(z)$.

We shall develop an algorithm to obtain \mathbf{V} . Let $v = \mu + \omega$. Our problem can be simply put as finding the variation \mathbf{V} as μ changes to v . Hence, $f^v = f^\mu + \mathbf{V}$.

Theorem 3 *Let f^μ and f^v be the quasi-conformal maps with Beltrami coefficients $\mu : \Omega_1 \rightarrow \mathbb{C}$ and $v : \Omega_1 \rightarrow \mathbb{C}$ respectively. Suppose $f^v = f^\mu + \mathbf{V}$. Let \mathcal{A} be the differential operator defined by $\mathcal{A} := \frac{\partial}{\partial \bar{z}} - v \frac{\partial}{\partial z}$. Then:*

$$\mathcal{A}\mathbf{V} = -\mathcal{A}f^\mu \tag{15}$$

Proof Since f^v is the quasi-conformal map with Beltrami coefficient $v : \Omega_1 \rightarrow \mathbb{C}$, $\frac{\partial f^v}{\partial \bar{z}} = v \frac{\partial f^v}{\partial z}$. Equivalently,

$$\mathcal{A}f^v = \left(\frac{\partial}{\partial \bar{z}} - v \frac{\partial}{\partial z} \right) f^v = 0. \tag{16}$$

Now, since $f^v = f^\mu + \mathbf{V}$, we obtain

$$\mathcal{A}f^v = \mathcal{A}(f^\mu + \mathbf{V}) \implies 0 = \mathcal{A}(f^\mu + \mathbf{V}) \tag{17}$$

Hence, $\mathcal{A}\mathbf{V} = -\mathcal{A}f^\mu$ as required. □

In other words, finding \mathbf{V} is equivalent to solving the partial differential equation (15) subject to the boundary condition that

$$(f^\mu + \mathbf{V})(\gamma_i) = \gamma'_i \text{ for } i = 0, 1, 2, \dots, n \tag{18}$$

Note that the point-wise correspondence between γ_i and γ'_i is not required in (18).

Using Theorem 3, we propose to iteratively deform f^μ to f^ν . More specifically, our goal is to obtain a sequence of quasi-conformal maps $\{f_n\}_{n=1}^\infty$ such that $f_0 = f^\mu$ and $f_\infty = f^\nu$. To do this, the basic idea is to flow μ to ν iteratively to obtain a sequence of Beltrami coefficients converging to ν . Their associated quasi-conformal maps are then computed by solving Eq. (15) to obtain $\{f_n\}_{n=1}^\infty$, which converges to $f_\infty = f^\nu$. The procedure can be illustrated in more details as follows:

$$\begin{array}{ccccccccccc}
 \mu_0 := \mu & \longrightarrow & \mu_1 & \longrightarrow & \dots & \longrightarrow & \mu_n & \longrightarrow & \dots & \longrightarrow & \mu_\infty = \nu \\
 \updownarrow & & \updownarrow & & & & \updownarrow & & & & \updownarrow \\
 f_0 := f^\mu & \longrightarrow & f_1 & \longrightarrow & \dots & \longrightarrow & f_n & \longrightarrow & \dots & \longrightarrow & f_\infty = f^\nu
 \end{array} \tag{19}$$

More specifically, we first set $f_0 = f^\mu$ and $\mu_0 = \mu$. We then flow f_0 to f_1 whose Beltrami coefficient is close to $\nu_1 := (1 - \epsilon)\mu_0 + \epsilon\nu$ ($\epsilon > 0$). This can be done by solving Eq. (15) by putting $\nu = \nu_1$ with the boundary constraint to obtain \mathbf{V}_0 . Note that \mathbf{V}_0 on the boundaries is restricted to be tangential to the boundary curves. We get a new quasi-conformal map $f_1 := f_0 + \mathbf{V}_0$ whose Beltrami coefficient is denoted by μ_1 .

Suppose at the n^{th} iteration, we have the quasi-conformal map f_n with Beltrami coefficient μ_n .

We then flow f_n to f_{n+1} whose Beltrami coefficient is close to $\nu_n := (1 - \epsilon)\mu_n + \epsilon\nu$ ($\epsilon > 0$). This is again done by solving Eq. (15) by putting $\nu = \nu_n$ and $f^\mu = f_n$ with the boundary constraint to obtain \mathbf{V}_n . Set $f_{n+1} := f_n + \mathbf{V}_n$ whose Beltrami coefficient is denoted by μ_{n+1} . Note that in each step, ϵ can be chosen so that $\|\mu_{n+1} - \nu\|_\infty$ is minimized.

In practice, we choose $\epsilon = 1$ and it works well for all our numerical experiments. A sequence of quasi-conformal maps $\{f_n\}_{n=1}^\infty$ is obtained, whose Beltrami coefficients converge to ν . We call such a process to deform f^μ to f^ν iteratively the *Beltrami holomorphic flow (BHF)* from μ to ν , and denote it by: $\mathbf{BHF}(\mu \rightarrow \nu)$. The numerical implementation of the BHF procedure will be explained in more details in Sect. 6.1.

The Beltrami holomorphic flow can be summarized as follows:

Algorithm 1 (*Beltrami holomorphic flow*)

Input: $f^\mu : \Omega_1 \rightarrow \Omega_2$ with Beltrami coefficient μ , target Beltrami coefficient ν

Output: Sequence of quasi-conformal maps $\{f_n\}_{n=1}^\infty$

1. Set $f_0 = f^\mu$. Solve Equation (15) to obtain \mathbf{V}_0 ;
2. Given f_n , compute $\mu_n := \mu(f_n)$ and $\nu_n := (1 - \epsilon)\mu_n + \epsilon\nu$; solve Equation (15) by putting $\nu = \nu_n$ and $f^\mu = f_n$ to obtain \mathbf{V}_n ; Set $f_{n+1} := f_n + \mathbf{V}_n$;
3. If $\|\mu_{n+1} - \mu_n\| \geq \epsilon'$, repeat step 2. Otherwise, stop the iteration.

5.2 Iteration Scheme for Computing T-Maps

In this subsection, we describe how we can obtain a sequence of BCs, $\{\nu_n\}_{n=1}^\infty$, which converges to the optimal ν^* associated to our desired extremal T-Map, f^* .

Given an initial map $f_0 : \Omega_1 \rightarrow \Omega_2$ such that $f_0(\gamma_i) = \gamma_i'$ ($i = 0, 1, 2, \dots, n$), let $\nu_0 = \mu(f_0)$ be the BC associated with f_0 . We proceed to iteratively adjust ν_0 to solve the optimization problem (13).

Recall that the optimal ν^* must be of Teichmüller type, according to Theorem 2. That is, $\nu^* \in \mathfrak{T}(\Omega_1, \Omega_2)$ where

$$\mathfrak{T}(\Omega_1, \Omega_2) := \left\{ \nu = k \frac{\bar{\varphi}}{|\varphi|} \mid 0 \leq k < 1, \varphi \text{ integrable holomorphic,} \right. \\
 \left. \nu = \mu(f) \text{ for some } f : \Omega_1 \rightarrow \Omega_2 \right\}$$

To find the desired T-Map, our strategy is to apply a simple iterative scheme over the space of $\mathfrak{T}(\Omega_1, \Omega_2)$ to minimize $E_2(v) = \|v\|_\infty$. According to Theorem 2, E_2 has a unique global minimizer which is in $\mathfrak{T}(\Omega_1, \Omega_2)$.

Thus, to obtain the global minimizer, we firstly adjust v to minimize E_2 over the space $\mathfrak{B}(\Omega_1, \Omega_2)$ of all Beltrami coefficients. We then project v into $\mathfrak{T}(\Omega_1, \Omega_2)$. A sequence of BCs can be obtained, whose supreme norms monotonically decreases to a global minimizer of E_2 . According to Theorem 2, the global minimizer exists and is unique. Hence, the sequence converges to an optimal BC, v^* , associated with our desired extremal T-Map, f^* .

More specifically, the proposed algorithm can be described as follows. Given v_0 , we first project it into the space of $\mathfrak{T}(\Omega_1, \Omega_2)$. To do this, we first normalize v_0 by an averaging operator:

$$\mathcal{N}(v) = \left(\frac{\int_{\Omega_1} |v| d\Omega_1}{A(\Omega_1)} \right) e^{i\theta} \tag{20}$$

where $\frac{v}{|v|} = e^{i\theta}$ and $A(\Omega_1) = \text{area of } \Omega_1$. Then, we apply a Laplace smoothing \mathcal{L} indedependently on $|\mathcal{N}(v_0)|$ and $\mathbf{arg}(\mathcal{N}(v_0))$.

The operators project v_0 to another BC. We next obtain a quasi-conformal map $g := \mathbf{BHF}(v_0 \rightarrow \mathcal{L}(\mathcal{N}(v_0)))$, whose BC is given by v , with the constraint that $g|_{\partial\Omega_1} = f_0|_{\partial\Omega_1}$. Note that v is generally not in $\mathfrak{T}(\Omega_1, \Omega_2)$. We repeat such a process and update g as follows: $g := \mathbf{BHF}(v \rightarrow \mathcal{L}(\mathcal{N}(v)))$. The process continues until $\|v \rightarrow \mathcal{L}(\mathcal{N}(v))\|_\infty < \epsilon$. This procedure iteratively adjusts the norm and the argument (or angles) of v such that v becomes an admissible BC of Teichmüller type. Eventually, we obtain a T-Map $g : \Omega_1 \rightarrow \Omega_2$, whose BC is of Teichmüller type. That is, $v \in \mathfrak{T}(\Omega_1, \Omega_2)$. We call this process the *projection* of v_0 into the space of $\mathfrak{T}(\Omega_1, \Omega_2)$, and denote it by $(v, g) = \mathcal{P}(v_0)$.

The existence of such a projection is theoretically guaranteed and its supreme norm must be less than $\|v_0\|_\infty$, according to Theorem 1. The convergence of the projection process can be established by an argument of the harmonic energy minimization (see Sect. 5.4). The algorithm of the projection can be summarized as follows:

Algorithm 2 (*Projection*)

Input: $\mu \in \mathfrak{B}(\Omega_1, \Omega_2)$

Output: *Projection, v , of μ into $\mathfrak{T}(\Omega_1, \Omega_2)$ and the corresponding quasi-conformal map g*

1. Compute $g_0 := \mathbf{BHF}(\mu \rightarrow \mathcal{L}(\mathcal{N}(\mu)))$ and $v_0 := \mu(g_0)$;
2. Given g_n , compute $g_{n+1} := \mathbf{BHF}(v_n \rightarrow \mathcal{L}(\mathcal{N}(v_n)))$ with $g_{n+1}|_{\partial\Omega_1} = f_n|_{\partial\Omega_1}$, and $v_{n+1} := \mu(g_{n+1})$;
3. If $\|v_{n+1} - \mathcal{L}(\mathcal{N}(v_{n+1}))\|_\infty \geq \epsilon$, repeat step 2. Otherwise, stop the iteration.

Now, to minimize $E_2(v) = \|v\|_\infty$, we perform a damping operation on v . More specifically, we diffuse v through

$$\frac{\partial v}{\partial t} = -v \tag{21}$$

We diffuse v over a finite time over $\mathfrak{B}(\Omega_1, \Omega_2)$, and denote the damping operation on v by $\mathcal{D}(v)$. It reduces $E_2(v) = \|v\|_\infty$.

A new map $g_1 : \Omega_1 \rightarrow \Omega_2$ can then be obtained through BHF:

$$g_1 := \mathbf{BHF}(v_0 \rightarrow \mathcal{D}(v_0)) \tag{22}$$

Let $\mu_1 := \mu(g_1)$. We project μ_1 into the space of $\mathfrak{T}(\Omega_1, \Omega_2)$ to get $(v_1, f_1) := \mathcal{P}(\mu_1)$. Thus, we obtain the T-Map f_1 , whose BC is v_1 . The iteration continues until it converges to the optimal v^* associated to the desired extremal T-Map f^* .

Therefore, given $f_n : \Omega_1 \rightarrow \Omega_2$ whose Beltrami coefficient is v_n , we adjust v_n and f_n as follows:

$$\begin{aligned} g_{n+1} &:= \mathbf{BHF}(v_n \rightarrow \mathcal{D}(v_n)) \\ \mu_{n+1} &:= \mu(g_{n+1}) \\ (v_{n+1}, f_{n+1}) &:= \mathcal{P}(\mu_{n+1}) \end{aligned} \tag{23}$$

As a result, we obtain a sequence of BCs $\{v_n\}_{n=1}^\infty$ whose supreme norm monotonically decreases. Hence, $\{v_n\}_{n=1}^\infty$ converges to an optimal v^* . Note that v^* must be a global minimizer of E_2 . Suppose not, then there exists an admissible $\mu \in \mathfrak{T}(\Omega_1, \Omega_2)$ whose supreme norm is smaller than that of v^* . Our algorithm, which damps the supreme norm of the BC, will continue to look for another BC, $\mu \in \mathfrak{T}(\Omega_1, \Omega_2)$, whose supreme norm is smaller than that of v^* . It contradicts that v^* is a limit point of the sequence. Hence, v^* must be a global minimizer of E_2 . Furthermore, according to Theorem 2, $E_2(v) = \|v\|_\infty$ has a unique global minimizer. We conclude that v^* is the unique BC associated to our desired extremal T-Map, f^* , which solves the optimization problem (13).

In summary, the iterative scheme for computing T-Maps can be described as follows:

Algorithm 3 (Iteration scheme for computing T-Maps)

Input: Multiply-connected domains Ω_1 and Ω_2 of the same topology

Output: Optimal Beltrami coefficient v^* and the extremal T-Map f^*

1. Obtain an initial map $f_0 : \Omega_1 \rightarrow \Omega_2$ with $f_0(\gamma_i) = \gamma_i'$ ($i = 0, 1, 2, \dots, n$). Set $v_0 = \mu(f_0)$;
2. Given v_n , compute $g_{n+1} := \mathbf{BHF}(v_n \rightarrow \mathcal{D}(v_n))$ and $\mu_{n+1} := \mu(g_{n+1})$; Project μ_{n+1} into $\mathfrak{T}(\Omega_1, \Omega_2)$ to obtain $(v_{n+1}, f_{n+1}) := \mathcal{P}(\mu_{n+1})$;
3. If $\|v_{n+1} - v_n\| \geq \epsilon$, repeat step 2. Otherwise, stop the iteration.

Remark 1 To better illustrate the idea of the algorithm, we consider the norm of the Beltrami coefficient on the circle $\{0.65e^{i\theta} : 0 \leq \theta \leq 2\pi\} \subset \Omega_1$ at each iterations as shown in Fig. 3a. Initially, we have an initial map f_0 associated with the Beltrami coefficient, μ_0 . The norm of μ_0 is not a constant everywhere. We project μ_0 to the space of $\mathfrak{T}(\Omega_1, \Omega_2)$ to obtain v_0 . Observe that the norm of v_0 is uniform everywhere. Using the damping operator, we minimize E_2 to get μ_1 with smaller supreme norm. By projection, we get $v_1 \in \mathfrak{T}(\Omega_1, \Omega_2)$,

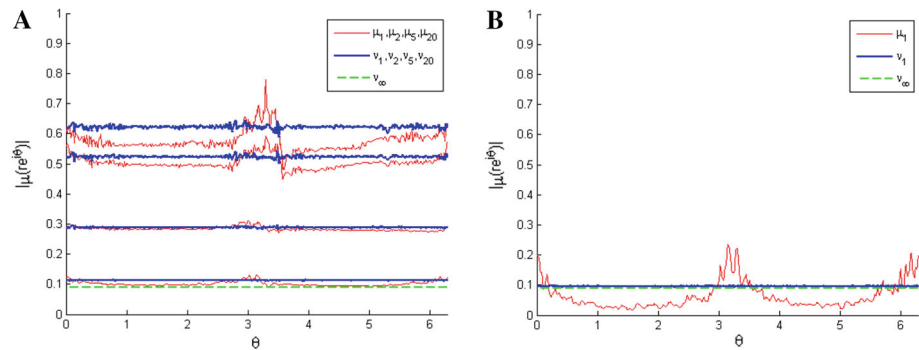


Fig. 3 **a** The norm of the Beltrami coefficient on the circle $\{0.65e^{i\theta} : 0 \leq \theta \leq 2\pi\}$ at each iterations with an arbitrary initialization. **b** The norm of the Beltrami coefficient on the circle $\{0.65e^{i\theta} : 0 \leq \theta \leq 2\pi\}$ at each iterations with the initialization introduced in Sect. 5.3

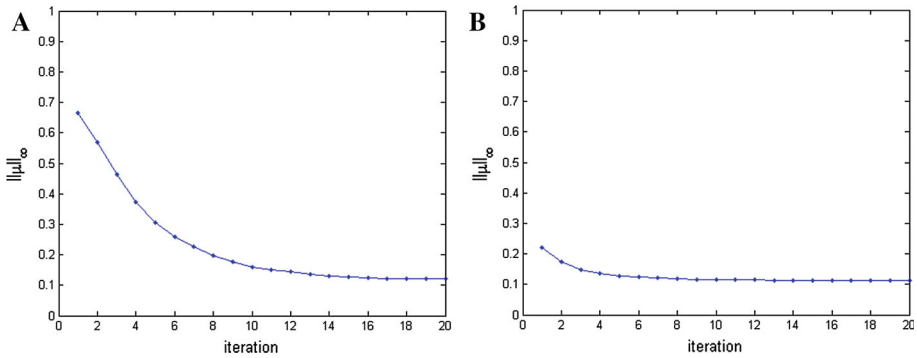


Fig. 4 Convergence of the proposed algorithm under different initializations. **a** The supreme norm of v_n versus iterations under an arbitrary initialization. The iterative scheme takes about 20 iterations to converge. **b** The supreme norm of v_n versus iterations under the initialization described in Sect. 5.3. The iterative scheme get to the optimal Beltrami coefficient quickly

which is of Teichmüller type, from μ_1 . The norm of v_1 is uniform everywhere and it is smaller than $\|\mu_1\|_\infty$. Eventually, we get a sequence of Beltrami coefficient $\{v_n\}_{n=1}^\infty$ such that $E_2(v_n) = \|v_n\|_\infty$ monotonically decreases (see Fig. 4a). The sequence converges to the optimal v^* associated with the desired extremal T-Map.

5.3 Initialization of the Iterative Scheme

The speed of convergence of the proposed algorithm depends on the initialization chosen. We propose to obtain a good initialization, f_0 , which is close to the optimal extremal T-Map. In this paper, the initial map f_0 is chosen so that its Beltrami coefficient is closest to $\mu = 0$ in the least square sense, using the Beltrami holomorphic flow. We first compute a harmonic map $h : \Omega_1 \rightarrow \Omega_2$ between Ω_1 and Ω_2 with arbitrary boundary correspondence. Let μ_h be the Beltrami coefficient of h . We can then obtain an initial map f_0 given by: $f_0 := \mathbf{BHF}(\mu_h \rightarrow \mu \equiv 0)$.

Numerical results show that with this initialization, the iterative scheme converges very fast. In Fig. 4a, we show the supreme norm of v_n versus iterations under an arbitrary initialization. The iterative scheme takes about 20 iterations to converge. In Fig. 4b, we perform the same experiment but using the initialization introduced in this subsection. The initialization is very close to the optimal minimizer and hence iterative scheme converges to the optimal Beltrami coefficient quickly. Despite different initializations are used, the iterative scheme converge to the same optimal BC. It illustrates that the extremal T-Map is unique.

Remark 2 In Fig. 3b, we again consider the norm of the Beltrami coefficient on the circle $\{0.65e^{i\theta} : 0 \leq \theta \leq 2\pi\} \subset \Omega_1$ at each iterations. When good initiation f_0 is chosen, its associated Beltrami coefficient μ_0 is very close to v^* . After projection of μ_0 to $\mathfrak{T}(\Omega_1, \Omega_2)$, the projected Beltrami coefficient $v_0 \in \mathfrak{T}(\Omega_1, \Omega_2)$ is very close to v^* . Hence, the algorithm converges quickly if initialization is carefully chosen.

5.4 Convergence Analysis

In this subsection, we will study the convergence of the proposed algorithms. Three algorithms are proposed in this paper. Algorithm 1, which is also called the Beltrami holomorphic

flow, computes the best quasi-conformal map whose BC is closest to the prescribed BC. Algorithm 2 or the projection operator projects an arbitrary BC to a BC of Teichmüller type. Algorithm 3, which is the main algorithm, computes the extremal T-Map between two multiply-connected domains. The algorithm produces a sequence of BCs, $\{v_n\}_{n=1}^\infty$ of Teichmüller type. We will show that the sequence converges to the optimal BC, v^* , associated with the unique extremal T-Map f^* .

One step in our main algorithm (Algorithm 3) is the projection of an arbitrary BC to a BC of Teichmüller type (Algorithm 2). We first explain why the projection operator \mathcal{P} works. Suppose a BC, μ_n , is obtained at the n^{th} iteration. We can show that v_n obtained from $\mathcal{P}(\mu_n)$ is indeed of the Teichmüller type and its associated quasi-conformal map f_n is a T-Map.

Let μ be an admissible BC, which is associated to a quasi-conformal map $g : \Omega_1 \rightarrow \Omega_2$. According to Theorem 1, there exists a unique T-Map f^* , subject to the boundary constraint $f^*|_{\Omega_1} = g|_{\Omega_1}$. The convergence of the projection operator on *general (open or closed) Riemann surfaces of arbitrary topologies* can be theoretically proven [16]. In [16], we discuss the theoretical proof of the convergence in details. We have the following key results. Basically, $\mathbf{BHF}(\mu \rightarrow \mathcal{L}(\mathcal{N}(\mu)))$ computes the generalized harmonic map under the auxiliary metric, $|dz + \mathcal{L}(\mathcal{N}(\mu))\overline{d\bar{z}}|^2$, given by the BC, $\mathcal{L}(\mathcal{N}(\mu))$. From Algorithm 2, we obtain a sequence of BCs, $\{\mu_n := \mathcal{L}(\mathcal{N}(v_n))\}_{n=1}^\infty$, where $v_n = \mu(f_n)$. In [16], we show that μ_n converges to an admissible BC, μ^* . Also, $\mu^* = v^* := \mu(f^*)$, where f^* is the optimal quasi-conformal map obtained and v^* is its associated BC. An important question is whether the algorithm converges to the unique admissible BC, v^* , of Teichmüller type, which is associated to a T-Map, f^* . This can be guaranteed due to the following observations.

Theorem 4 (Convergence of the projection operator) *Algorithm 2 gives a convergent sequence of pairs (v_n, f_n) , where v_n is the Beltrami coefficient of f_n , whose limit point is (v^*, f^*) . Here, v^* is the unique admissible Beltrami coefficient of Teichmüller type associated with the T-Map.*

Proof Suppose (f_n, v_n) is obtained at the n -th iteration. $f_n = \mathbf{BHF}(v_{n-1} \rightarrow \mu_n)$, where $\mu_n := \mathcal{L}(\mathcal{N}(v_{n-1}))$. Note that the BC of f_n is generally not equal to μ_n . In fact, f_n is the harmonic map between Ω_1 and Ω_2 under the auxiliary metric, $g(\mu_n) = |dz + \mu_n \overline{d\bar{z}}|^2$. An energy functional E_{BC} can then be defined on the space of all BCs, $\mathcal{B}(\Omega_1)$, by letting $E_{BC}(\mu)$ be the harmonic energy of the generalized harmonic map under the auxiliary metric $g(\mu)$. In [16], we prove that $E_{BC}(\mu) \geq A_2$ ($=$ area of Ω_2) and equality holds if and only if μ is admissible. It is also proven that μ_n converges to a minimizer of E_{BC} , μ^* . Since E_{BC} attains its minimum at μ^* when μ^* is admissible, it implies the QC iteration converges to a pair (f^*, v^*) , where $v^* = \mu(f^*) = \mu^*$.

Next, we show that v^* is of Teichmüller type. At each step of the QC iteration, a Laplace smoothing \mathcal{L} and averaging \mathcal{N} are applied on v_n . At the optimal state, $\mathcal{L}(\mathcal{N}(v^*)) = v^*$. This implies that $\Delta(\mathbf{arg}(v^*)) = 0$ and $|v^*| = k$, where k is a positive constant. Since $\mathbf{arg}(v^*)$ is harmonic, there exists a harmonic conjugate ζ of $\mathbf{arg}(v^*)$ such that $\zeta - i\mathbf{arg}(v^*)$ is holomorphic. Let $\varphi = e^{\zeta - i\mathbf{arg}(v^*)}$. φ is holomorphic and $v^* = k \frac{\overline{\varphi}}{|\varphi|}$. Hence, v^* is an admissible BC of Teichmüller type. By Theorem 1, given the prescribed boundary constraints, there exists only one admissible BC of Teichmüller type. We conclude that v^* is the unique BC associated to the unique extremal T-Map. □

Therefore, Algorithm 3 gives us a sequence of BCs, $\{v_n\}_{n=1}^\infty$, of Teichmüller type. A question is whether the supreme norm of v_n is indeed decreasing, so that an extremal T-Map can be obtained at the optimal state. Suppose at the n^{th} iteration in Algorithm 3, (v_n, f_n) is obtained, where v_n is the BC of f_n . The damping operator \mathcal{D} is applied to v_n to reduce

the supreme norm of v_n . In fact, the damping operator diffuse v_n to $\mathcal{D}(v_n)$ through equation (21). Thus, $\mathcal{D}(v_n) = e^{-t}v_n$ for some $t > 0$, and $\|\mathcal{D}(v_n)\|_\infty = e^{-t}\|v_n\|_\infty < \|v_n\|_\infty$. Now, $g_{n+1} = \mathbf{BHF}(v_n \rightarrow \mathcal{D}(v_n))$ looks for a quasi-conformal map g_n , whose BC μ_{n+1} is closest to v_n . Stricly speaking, the Beltrami Holomorphic Flow (BHF) in Sect. 5.1 can be stated as follow:

$$\mathbf{BHF}(\mu \rightarrow \nu) = \mathbf{argmin}_f \left\| \frac{\partial f}{\partial \bar{z}} / \frac{\partial f}{\partial z} - \nu \right\|_\infty \tag{24}$$

It can be solved numerically by minimizing $\|\frac{\partial f}{\partial \bar{z}} / \frac{\partial f}{\partial z} - \nu\|_p^p$ for sufficiently large p using gradient descent. In our actual implementation, we minimize $\|\frac{\partial f}{\partial \bar{z}} - \nu \frac{\partial f}{\partial z}\|_2^2$ instead. However, it is found that the performance is already satisfactory. Since $\|\mathcal{D}(v_n)\|_\infty < \|v_n\|_\infty$ and $g_{n+1} = \mathbf{BHF}(v_n \rightarrow \mathcal{D}(v_n))$, then the supreme norm of the BC of g_{n+1} is less than that of v_n . In other words, $\|\mu_{n+1}\|_\infty < \|v_n\|_\infty$.

Note that μ_n is in general not of Teichmüller type. We then apply the projection operator on μ_n to obtain $(v_{n+1}, f_{n+1}) := \mathcal{P}(\mu_{n+1})$.

Now, the final question is whether the supreme norm of the BC after projection would still decrease. In other words, we need to show that $\|v_{n+1}\|_\infty < \|v_n\|_\infty$. This can be guaranteed by the following theorem.

Theorem 5 *Suppose (v_n, f_n) is obtained at the n^{th} iteration of Algorithm 3. Let $g_{n+1} = \mathbf{BHF}(v_n \rightarrow \mathcal{D}(v_n))$. Then, $\|v_{n+1}\|_\infty < \|v_n\|_\infty$, where $(v_{n+1}, f_{n+1}) := \mathcal{P}(\mu_{n+1})$.*

Proof v_{n+1} and f_{n+1} are obtained from the projection operator $\mathcal{P}(\mu_{n+1})$, where v_{n+1} is the BC of f_{n+1} . According to Theorem 1, $f_{n+1} : \Omega_1 \rightarrow \Omega_2$ is the unique T-Map with the boundary condition that $f_{n+1}|_{\Omega_1} = g_{n+1}|_{\Omega_1}$. Thus, $K(f_{n+1}) \leq K(g_{n+1})$ and equality holds if and only if $f_{n+1} = g_{n+1}$. This implies $\|v_{n+1}\|_\infty \leq \|\mu_{n+1}\|_\infty$ (equality holds if and only if $f_{n+1} = g_{n+1}$). Now, since $\|\mu_{n+1}\|_\infty < \|v_n\|_\infty$, we conclude that $\|v_{n+1}\|_\infty < \|v_n\|_\infty$. \square

In summary, Algorithm 3 gives a sequence of BCs, $\{v_n\}_{n=1}^\infty$, of Teichmüller type, whose supreme norm decreases as n increases. Each v_n is associated to a T-Map f_n , and f_n converges to our desired extremal T-Map. In the rare situation when the iterations get stuck at the local minimum of the energy functional (13), one can apply L^p (instead of L^2) minimization in Algorithm 1 with large p . The obtained sequence would converge to the global minimizer.

6 Numerical Implementation

In this section, we will explain in detail the numerical implementation of the algorithms proposed in Sect. 5.

In practice, multiply-connected 2D domains or surfaces in \mathbb{R}^3 are usually represented discretely by triangular meshes. Suppose K_1 and K_2 are two meshes with the same topology representing Ω_1 and Ω_2 . We define the set of vertices on K_1 and K_2 by $V^1 = \{v_i^1\}_{i=1}^n$ and $V^2 = \{v_i^2\}_{i=1}^n$ respectively. Similarly, we define the set of triangular faces on K_1 and K_2 by $F^1 = \{T_j^1\}_{j=1}^m$ and $F^2 = \{T_j^2\}_{j=1}^m$. Our goal is to look for a piecewise linear homeomorphism between K_1 and K_2 that approximates the extremal T-Map between Ω_1 and Ω_2 .

6.1 Implementation Details of BHF

The major step in computing the Beltrami holomorphic flow as described in Algorithm 5.1 is to solve Eq. (15). We first discretize the operator \mathcal{A} in Eq. (15). Let $f = (u + \sqrt{-1}v) : K_1 \rightarrow$

K_2 . To compute \mathcal{A} , we simply need to approximate the partial derivatives at each face T . We denote them by $D_x f = D_x u + \sqrt{-1}D_x v$ and $D_y f = D_y u + \sqrt{-1}D_y v$ respectively. Note that f is piecewise linear. The restriction of f on each triangular face T can be written as:

$$f|_T(x, y) = \begin{pmatrix} a_T x + b_T y + r_T \\ c_T x + d_T y + s_T \end{pmatrix} \tag{25}$$

Clearly, $D_x u(T) = a_T$, $D_y u(T) = b_T$, $D_x v(T) = c_T$ and $D_y v(T) = d_T$. Now, the gradient $\nabla_T f := (D_x f(T), D_y f(T))^t$ on each face T can be computed by solving the linear system:

$$\begin{pmatrix} \mathbf{v}_1 - \mathbf{v}_0 \\ \mathbf{v}_2 - \mathbf{v}_0 \end{pmatrix} \nabla_T f = \begin{pmatrix} \frac{f(\mathbf{v}_1) - f(\mathbf{v}_0)}{|\mathbf{v}_1 - \mathbf{v}_0|} \\ \frac{f(\mathbf{v}_2) - f(\mathbf{v}_0)}{|\mathbf{v}_2 - \mathbf{v}_0|} \end{pmatrix}, \tag{26}$$

where $[\mathbf{v}_0, \mathbf{v}_1]$ and $[\mathbf{v}_0, \mathbf{v}_2]$ are two edges on T . By solving Eq. (26), a_T , b_T , c_T and d_T can be obtained. Hence on each face T ,

$$\nabla_T f = \frac{1}{2A} \sum_{j=1}^3 f(\mathbf{v}_j) \mathbf{s}_j, \tag{27}$$

where A is the area of T and

$$\begin{aligned} \mathbf{s}_1(T) &= \mathbf{n} \times (\mathbf{v}_3 - \mathbf{v}_2) \\ \mathbf{s}_2(T) &= \mathbf{n} \times (\mathbf{v}_1 - \mathbf{v}_3) \\ \mathbf{s}_3(T) &= \mathbf{n} \times (\mathbf{v}_2 - \mathbf{v}_1), \end{aligned} \tag{28}$$

where \mathbf{n} is the unit normal of T . Let $v(T)$ be a constant over the face T . Using the relations $\frac{\partial}{\partial \bar{z}} = (D_x - \sqrt{-1}D_y)/2$ and $\frac{\partial}{\partial z} = (D_x + \sqrt{-1}D_y)/2$, the operator \mathcal{A} can be discretized on each face T as follows:

$$\mathcal{A}f(T) = \frac{1}{4A}(1 - v(T), \sqrt{-1} + \sqrt{-1}v(T)) \sum_{j=1}^3 f(\mathbf{v}_j) \mathbf{s}_j. \tag{29}$$

Note that the right hand side of the above equation is linear in every $u(\mathbf{v}_j)$ and $v(\mathbf{v}_j)$, $j = 1, 2, 3$. Hence, the above discretization of \mathcal{A} transforms (15) into a linear system of $\{\mathbf{V}(\mathbf{v}_i^1)\}_{i=1}^n$. Let $\mathbf{V}(\mathbf{v}_i^1) = (P_i, Q_i)^t$ and $f^\mu(\mathbf{v}_i^1) = u_i + \sqrt{-1}v_i$, then for each face T_j , $j = 1, \dots, m$, we have

$$\begin{aligned} &\frac{1}{4\text{Area}(T_j)} \left(1 - v(T_j), \sqrt{-1} + \sqrt{-1}v(T_j)\right) \sum_{i=1}^3 \left(P_{T_j(i)} + \sqrt{-1}Q_{T_j(i)}\right) \mathbf{s}_i(T_j) \\ &= -\frac{1}{4\text{Area}(T_j)} \left(1 - v(T_j), \sqrt{-1} + \sqrt{-1}v(T_j)\right) \sum_{i=1}^3 \left(u_{T_j(i)} + \sqrt{-1}v_{T_j(i)}\right) \mathbf{s}_i(T_j), \end{aligned} \tag{30}$$

where $T_j(i)$ are the indices of the vertices of T_j , i.e. $T_j = [\mathbf{v}_{T_j(1)}^1, \mathbf{v}_{T_j(2)}^1, \mathbf{v}_{T_j(3)}^1]$.

Secondly, the boundary constraint (18) can be approximated by a linear constraint, so that the least square method can be applied to solve the problem. For each boundary vertex $\mathbf{v}_i^1 \in \gamma_j$, we only require $\mathbf{V}(\mathbf{v}_i^1)$ to be tangential to γ_j' at $f^\mu(\mathbf{v}_i)$. That is, if $\mathbf{V}(\mathbf{v}_i^1) = (P_i, Q_i)^t$ and $(a_i, b_i)^t$ is the direction of the tangent, then

$$b_i P_i - a_i Q_i = 0, \tag{31}$$

which is a linear constraint. The linear system (30) together with the constraint (31) may be overdetermined. Therefore we solve the system by least square method. For each iteration of Algorithm 5.1, $\mathbf{V}_n(\mathbf{v}_i^1)$ is solved as above. Set $\tilde{f}_{n+1}(\mathbf{v}_i^1) := f_n(\mathbf{v}_i^1) + \mathbf{V}_n(\mathbf{v}_i^1)$. For each boundary vertex $\mathbf{v}_i^1 \in \gamma_j$, it is not necessary that $\tilde{f}_{n+1}(\mathbf{v}_i^1) \in \gamma'_j$ because the boundary constraints are approximated. Nevertheless, when $\|v_n - \mu_n\|_\infty$ is sufficiently small, $\tilde{f}_{n+1}(\mathbf{v}_i^1)$ shall not be far away from γ'_j . Hence we can project $\tilde{f}_{n+1}(\mathbf{v}_i^1)$ onto γ'_j and obtain the solution $f_{n+1}(\mathbf{v}_i^1)$ such that $f_{n+1}(\gamma_j) = \gamma'_j$, i.e.

$$f_{n+1}(\mathbf{v}_i^1) := \mathbf{argmin}_{\mathbf{z} \in \gamma'_j} \|\tilde{f}_{n+1}(\mathbf{v}_i^1) - \mathbf{z}\|_2. \tag{32}$$

6.2 Implementation Details of the Iterative Scheme

The main operators involved in the iterative scheme proposed in Sect. (5.2) are: **BHF**($\mu \rightarrow v$), \mathcal{D} and \mathcal{P} . The numerical implementation of **BHF**($\mu \rightarrow v$) was described in the last subsection. We now describe the numerical implementation of \mathcal{D} and \mathcal{P} in detail.

Recall that the damping operator $\mathcal{D}(v)$ diffuses v through $\frac{\partial v}{\partial t} = -v$. In the discrete case, we define the damping operator as follows:

$$\mathfrak{D}(v)(T) := v(T) - \epsilon v(T) \tag{33}$$

where T is a triangular face of K_1 , $\epsilon > 0$.

Other operators are the averaging operator $\mathcal{N}(v)$ and the Laplace smoothing operator $\mathcal{L}(v)$. In the discrete case, the averaging operator is defined as follows:

$$\mathcal{N}(v)(T) := \left(\frac{\sum_{T' \in F^1} \text{Area}(T')|v(T')|}{\sum_{T' \in F^1} \text{Area}(T')} \right) \frac{v(T)}{|v(T)|} \tag{34}$$

where T is a triangular face of K_1 . Meanwhile, the Laplace smoothing operator is defined as:

$$\mathcal{L}(v)(T) := L(T)e^{i\theta(T)}, \tag{35}$$

where

$$L(T) := \sum_{T_i \in \text{Nbhd}(T)} \frac{|v(T_i)|}{|\text{Nbhd}(T)|} \text{ and } \theta(T) := \sum_{T_i \in \text{Nbhd}(T)} \frac{\mathbf{arg}(v(T_i))}{|\text{Nbhd}(T)|}. \tag{36}$$

7 Numerical Experiments

We have tested our proposed algorithms on synthetic data together with real 3D surface data obtained from the 3D scanner. All experiments have been carried out on a laptop with an Intel Core i7 2.10 GHz CPU and 12GB RAM.

7.1 Numerical Experiments of BHF

Example 1 We first examine the performance of BHF to iteratively compute a quasi-conformal map $f : \Omega_1 \rightarrow \Omega_2$ with a prescribed BC. We choose Ω_1 to be a triply-connected circle domain defined as:

$$\Omega_1 := \mathbb{D} \setminus (B_{0.26}(0.4 - 0.02i) \cup B_{0.16}(-0.32 + 0.09i)).$$

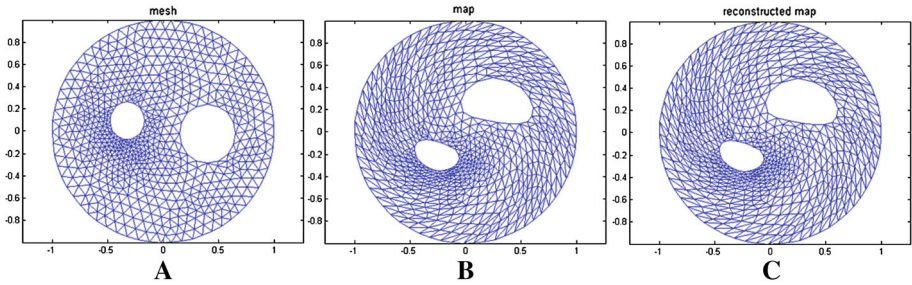


Fig. 5 a, b Two triply-connected domains. A quasi-conformal map f between (a) and (b) is given and its associated Beltrami coefficient is μ_f . c The reconstructed map obtained from μ_f using BHF

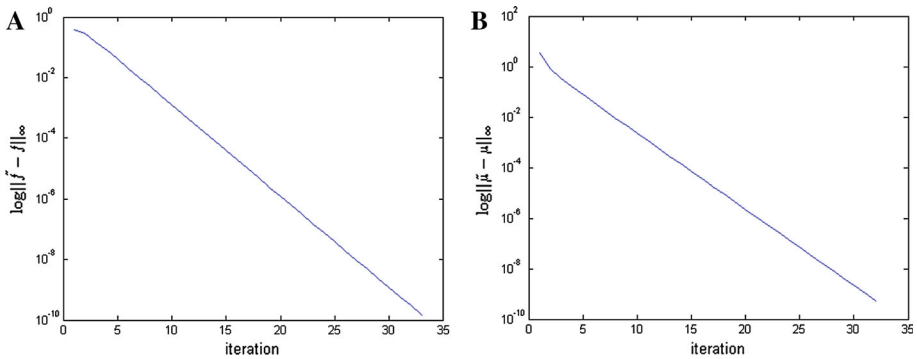


Fig. 6 a The error in coordinates $\|f - f_n\|_\infty$ versus iterations of the experiment in Fig. 5. b The error in BC $\|\mu_f - \mu(f_n)\|_\infty$ versus iterations

Ω_2 is chosen to be another triply-connected domain. In Fig. 5a, b shows two triply-connected domains. Given a quasi-conformal map f between (a) and (b), we obtain a Beltrami coefficient μ_f (defined on each triangular faces) corresponding to f . Using BHF, we can reconstruct the map f from μ_f . (c) shows the reconstructed map, which closely resembles to the original one. Figure 6a, b show the error in coordinates $\|f - f_n\|_\infty$ and error in BC $\|\mu_f - \mu(f_n)\|_\infty$ versus iterations respectively. Both converge to 0 quickly in less than 10 iterations.

Example 2 We repeat the experiment to compute the quasi-conformal map $f : \Omega_1 \rightarrow \Omega_2$ between two circle domains with three holes using BHF. Ω_1 is chosen to be:

$$\Omega_1 := \mathbb{D} \setminus (B_{0.16}(-0.11 - 0.46i) \cup B_{0.14}(-0.34 + 0.37i) \cup B_{0.18}(0.36 + 0.01i)).$$

Ω_2 is chosen to be another multiply-connected domain with three inner holes. Figure 7a, b shows two domains with three holes. We compute the Beltrami coefficient μ_f corresponding (defined on each triangular faces) to f . Using BHF, we reconstruct f from μ_f . (c) shows the reconstructed map, which closely resembles to the original one. Figure 8 shows the error in coordinates $\|f - f_n\|_\infty$ and error in BC $\|\mu_f - \mu(f_n)\|_\infty$ versus iterations. Again, both converge to 0 quickly in less than 10 iterations.

Example 3 In this example, we test whether the quasi-conformal map computed by BHF converges to the continuous quasi-conformal map as mesh size tends to 0. We consider:

$$\Omega_1 := \mathbb{D} \setminus (B_{0.1}(0.5i) \cup B_{0.1}(-0.4 - 0.3i) \cup B_{0.1}(0.4 - 0.3i)).$$

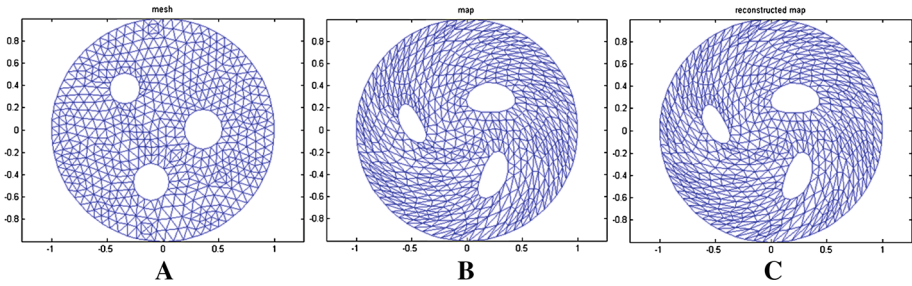


Fig. 7 a, b Two circle domains with three holes. A quasi-conformal map f between (a) and (b) is given and its associated Beltrami coefficient is μ_f . c The reconstructed map obtained from μ_f using BHF

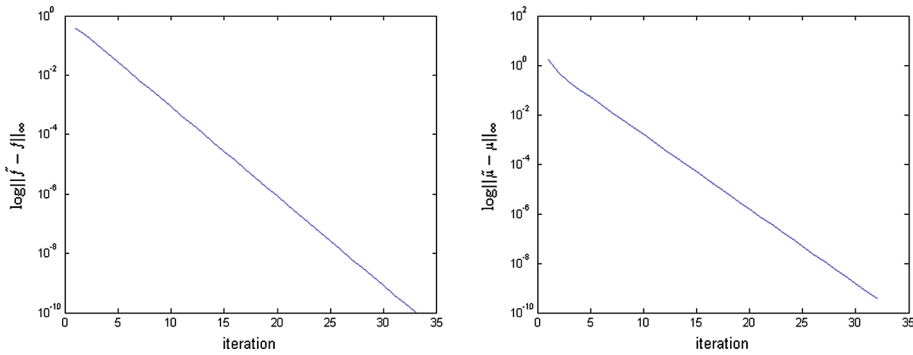


Fig. 8 a The error in coordinates $\|f - f_n\|_\infty$ versus iterations of the experiment in Fig. 11. b The error in BC $\|\mu_f - \mu(f_n)\|_\infty$ versus iterations

Ω_1 is deformed to Ω_2 through a diffeomorphism f given by:

$$f = e^{1.5i} z e^{1.5i|z|}, \text{ where } z = x + iy \tag{37}$$

Since f is a diffeomorphism, $\Omega_2 = f(\Omega_1)$ is a multiply-connected domain with three inner holes. The Beltrami coefficient of f can be explicitly computed, which is given by:

$$\mu_f = \left(\frac{-3i}{4} z^2 \right) / \left(|z| - \frac{3i}{4} |z|^2 \right) \tag{38}$$

The quasi-conformal map f is as shown in Fig. 9, which is visualized a texture mapping. Using different mesh size h , we approximate f using BHF. Figure 10a shows the log error of the BC versus the log of the mesh size. The error decreases as the mesh size decreases with a rate equal to 1.79. (b) shows the log error of the coordinates versus mesh size. The error again decreases as the mesh size decreases with a rate equal to 0.92.

7.2 T-Maps Between 2D Multiply-Connected Domains

Example 4 We test our proposed iterative scheme to compute the extremal T-Map on synthetic 2D multiply-connected domains. In Fig. 11, we compute the extremal T-map between two multiply-connected domains with three holes. We consider:

$$\begin{aligned} \Omega_1 &:= \mathbb{D} \setminus (B_{0.1}(0.33i) \cup B_{0.067}(0.33 - 0.33i) \cup B_{0.133}(-0.33 - 0.33i)); \\ \Omega_2 &:= \mathbb{D} \setminus (B_{0.1}(0.6i) \cup B_{0.1}(0.7 - 0.3i) \cup B_{0.1}(-0.7 - 0.3i)). \end{aligned}$$

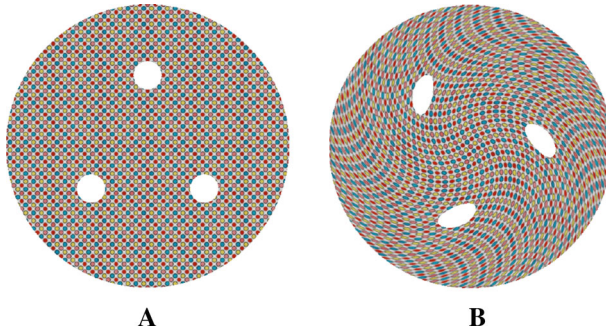


Fig. 9 The quasi-conformal map f in Example 3, visualized using texture mapping. **a** The domain Ω_1 and **b** The mapping $f(\Omega_1)$

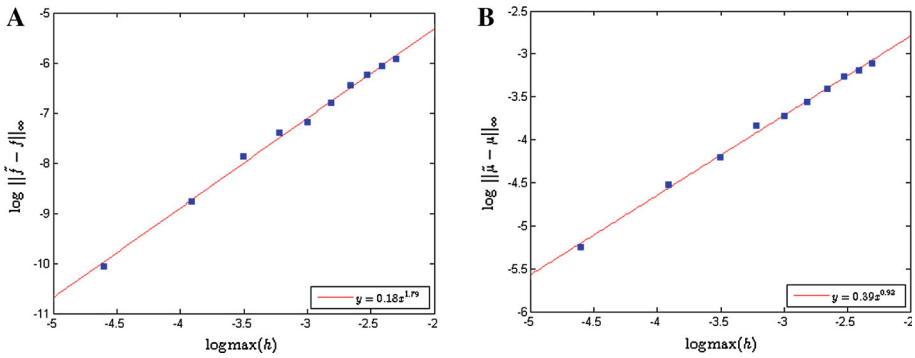


Fig. 10 Convergence of BHF to the continuous quasi-conformal map (described in Example 3) as mesh size tends to 0. **a** The log error of the coordinates versus the log of the mesh size. **b** The log error of the BC versus the log of the mesh size

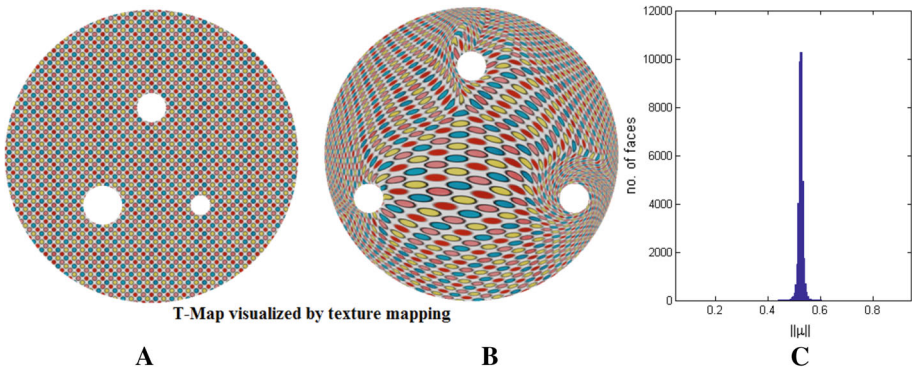


Fig. 11 **a, b** The two multiply-connected domains with three holes. The obtained extremal T-Map is visualized by texture mapping. The small circles on **(a)** are mapped to small ellipses on **(b)** under the extremal T-Map, with the same eccentricity. **c** The histogram of the norm of the BC

(a) and **(b)** shows the two multiply-connected domains Ω_1 and Ω_2 . The obtained extremal T-Map is visualized using texture mapping. The small circles on **(a)** are mapped to small ellipses on **(b)** under the extremal T-Map, with uniform eccentricity. In **(c)**, we show the

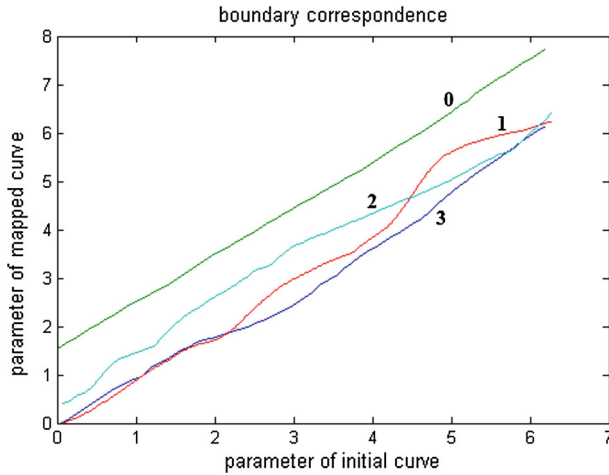


Fig. 12 This figure shows the boundary correspondence for each boundary component, plotted as a monotonic function defined on $[0, 2\pi]$

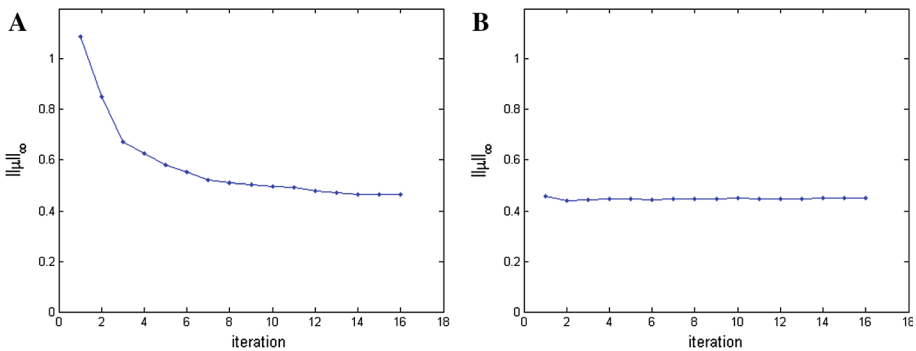


Fig. 13 **a** The energy $E_2(\mu(f_n)) := \|\mu(f_n)\|_\infty$ versus each iterations of Example 4 with an arbitrary initialization. **b** The energy $E_2(\mu(f_n)) := \|\mu(f_n)\|_\infty$ versus each iterations with the initialization proposed in Sect. 5.3

histogram of the norm of the BC. It accumulates at 0.53, meaning that the conformality distortion is uniform over the whole domain. It illustrates that the computed extremal map is indeed a T-Map.

Our proposed algorithm automatically determines the optimal boundary correspondence such that the conformality distortion is minimized. Figure 12 shows the boundary correspondence for each boundary component, plotted as a monotonic function defined on $[0, 2\pi]$.

Figure 13 shows the energy $E_2(\mu(f_n)) := \|\mu(f_n)\|_\infty$ versus each iterations with different initializations. Figure 13a shows the energy versus each iterations with an arbitrary initialization. Our proposed algorithm converges to the optimal BC with about 30 iterations. Using the initialization proposed in Sect. 5.3, the algorithm converges quickly. Figure 13a shows the energy versus each iterations with the good initialization. Note that the initial map is already close to the optimal one.

Example 5 In this example, we study the convergence of our proposed method to compute the extremal T-Map as mesh size tends to 0. We consider:

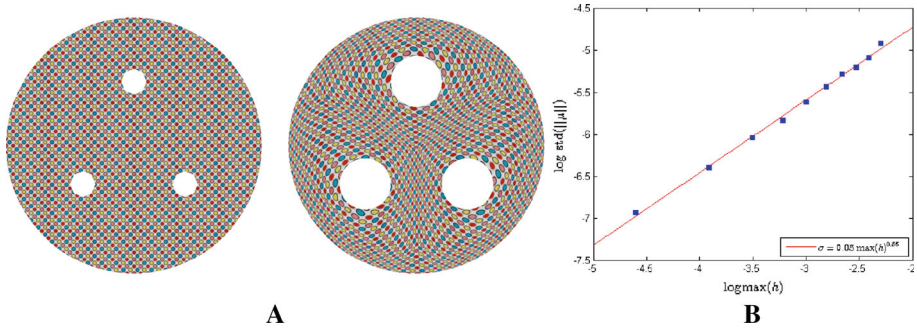


Fig. 14 **a** Two multiply-connected domains with three inner disks removed. We compute the extremal T-Map between them. **b** The log of the standard deviation of the BC norm versus the log of the mesh size h

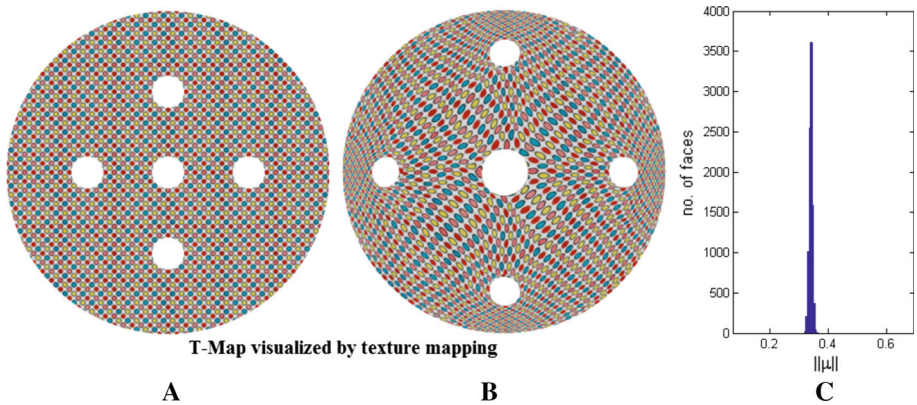


Fig. 15 **a, b** Two multiply-connected domains with five holes. The obtained extremal T-Map is visualized by texture mapping. The small circles on **(a)** are mapped to small ellipses on **(b)** under the extremal T-Map, with uniform eccentricity. **c** The histogram of the norm of the BC

$$\Omega_1 := \mathbb{D} \setminus (B_{0.1}(0.5i) \cup B_{0.1}(-0.4 - 0.3i) \cup B_{0.1}(0.4 - 0.3i));$$

$$\Omega_2 := \mathbb{D} \setminus (B_{0.2}(0.5i) \cup B_{0.2}(-0.4 - 0.3i) \cup B_{0.2}(0.4 - 0.3i)).$$

Figure 14a shows two multiply-connected domains with three inner disks removed. We proceed to compute the extremal T-Map between them with different mesh size. The standard deviation, $std(|v_h|)$ of the BC norm for each mesh size h is then computed. Figure 14b plots the log of the standard deviation $\log(std(|v_h|))$ versus the log of the mesh size h . It shows that the computed T-Map using our proposed method converges to the smooth T-Map as mesh size tends to 0. The convergence rate is about 0.86.

Example 6 We also test the algorithm on synthetic circle domains with more holes. Figure 15 shows the extremal T-map between two multiply-connected domains with 5 holes obtained by our proposed method. The histogram of the BC norm is shown in (c), which shows that the conformality distortion is uniform everywhere.

Example 7 In Fig. 16, we test our method on circle domains with 9 holes. (b) shows the obtained extremal T-Map visualized by texture mapping. The histogram of the BC norm is shown in (c), which means the obtained map is indeed a T-Map. This example demonstrates the effectiveness of our algorithm even on complicated domains with many holes.

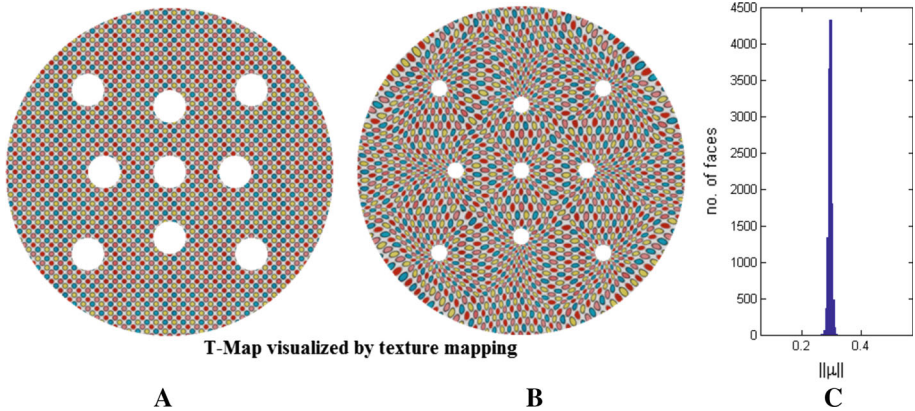


Fig. 16 **a, b** Two multiply-connected domains with nine holes. The obtained extremal T-Map is visualized by texture mapping. The small circles on **(a)** are mapped to small ellipses on **(b)** under the extremal T-Map, with uniform eccentricity. **c** The histogram of the norm of the BC

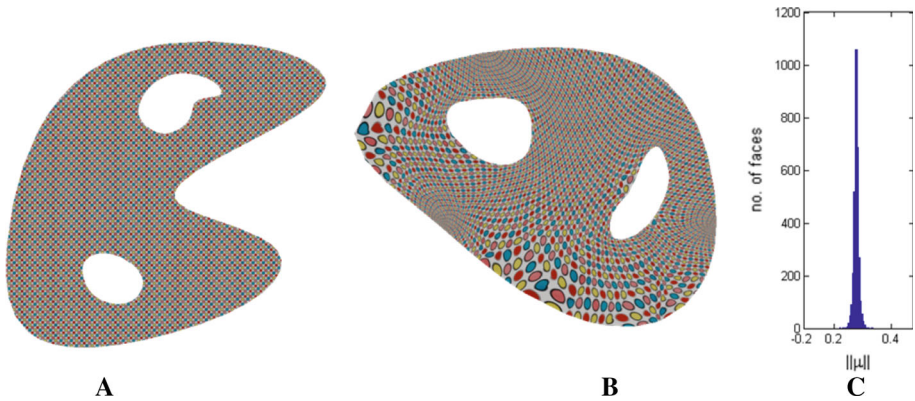


Fig. 17 **a, b** Two multiply-connected domains of arbitrary shapes with two holes. The obtained extremal T-Map is visualized by texture mapping. The small circles on **(a)** are mapped to small ellipses on **(b)** under the extremal T-Map, with uniform eccentricity. **c** The histogram of the norm of the BC

Example 8 In this experiment, we test our method to compute extremal T-Map between multiply-connected domains with arbitrary shapes (not restricted to circle domains). Figure 17 shows the computed extremal T-map between two multiply-connected domains of arbitrary shapes with two holes, visualized by texture mapping. Again, the histogram of the BC norm (as shown in (c)) shows that the conformality distortion is uniform everywhere, meaning that the extremal map is indeed of Teichmüller type.

Example 9 In this experiment, we test the efficiency of our method. We consider 7 pairs of multiply-connected domains and compute the extremal T-Map between them. The time to obtain the extremal T-Map is recorded in Table 1. The computation of all examples can be done within 1.5 minutes.

Example 10 In Fig. 18, we test our algorithm to compute extremal T-Map between two multiply-connected domains with significant different sizes of the inner holes. The obtained extremal T-Map is visualized by texture mapping. The histogram of the norm of the associated BC is shown in (c), which illustrates the computed map is indeed a T-Map.

Table 1 The elapsed time of the proposed algorithm for computing the extremal T-Maps in different examples

Number of vertices	Number of faces	Elapsed time (s)	$\ \mu\ _\infty$
22,160	43,115	87.7018	0.330403
17,746	35,008	73.0281	0.446511
17,746	35,008	62.6791	0.091014
6,282	12,141	19.9097	0.343128
4,832	9,376	7.6386	0.378116
671	1,240	0.9367	0.039436
588	1,056	1.3129	0.073473

The stopping criteria is $\|\mu(f_{n+1}) - \mu(f_n)\|_\infty < 10^{-3}$. $\|\mu(f^*)\|_\infty$ of the convergent results are also listed

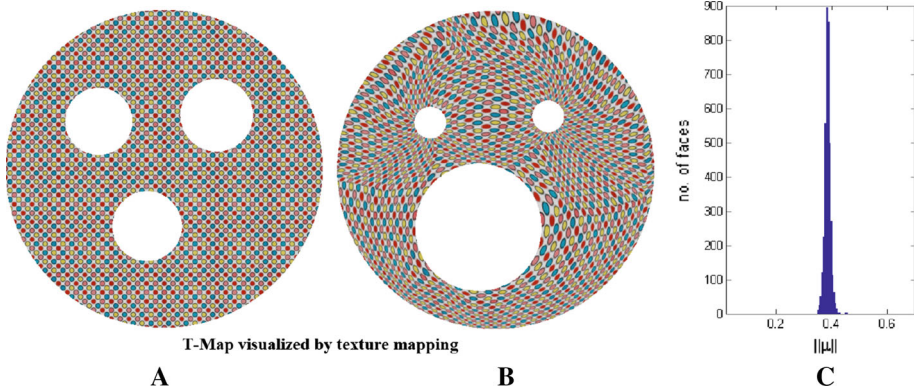


Fig. 18 a, b Two multiply-connected domains with significant different sizes of holes. The obtained extremal T-Map is visualized by texture mapping. The small circles on (a) are mapped to small ellipses on (b) under the extremal T-Map, with uniform eccentricity. c The histogram of the norm of the BC

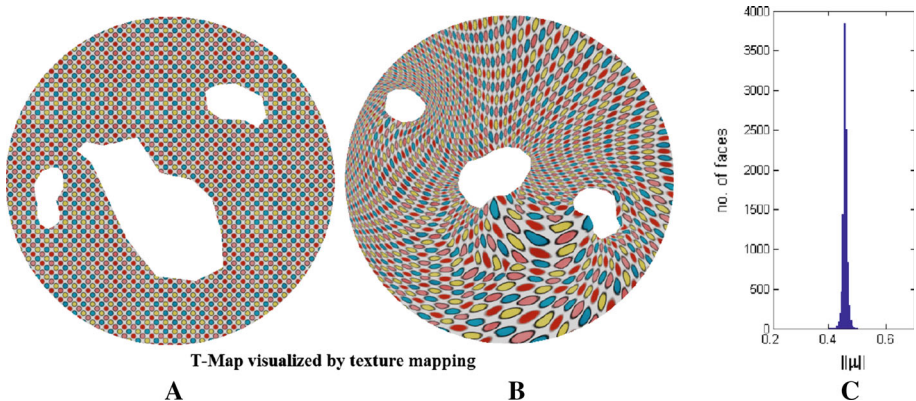


Fig. 19 a, b Two multiply-connected domains with different shapes of inner punctures. The obtained extremal T-Map is visualized by texture mapping. The small circles on (a) are mapped to small ellipses on (b) under the extremal T-Map, with uniform eccentricity. c The histogram of the norm of the BC

Example 11 In Fig. 19, we test our algorithm to compute extremal T-Map between two multiply-connected domains with different shapes of inner punctures. The obtained extremal T-Map is visualized by texture mapping. The histogram of the norm of the associated BC is

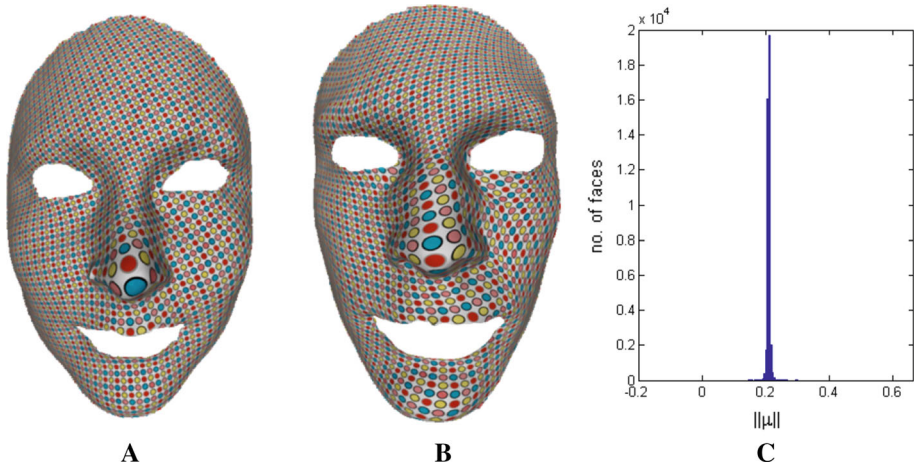


Fig. 20 **a, b** Two multiply-connected human faces. The extremal T-Map between them is computed, which is visualized using texture mapping. **c** The histogram of the norm of the BC

shown in (c), which illustrates the computed map is indeed a T-Map. This example demonstrates that our proposed method perform well on multiply-connected domains with complicated geometry.

7.3 T-Maps Between Multiply-Connected Surfaces

The proposed method can be easily extended to compute extremal T-Map between general multiply-connected surfaces through conformal parameterization. We test the proposed method to compute extremal map between multiply-connected 3D human faces. We also apply the algorithm to obtain the extremal parameterization of the human face onto a simple user-defined parameter domain, which is important for grid generation.

Example 12 Figure 20a, b shows two multiply-connected human faces. The extremal T-Map between them is computed, which is visualized using texture mapping. The small circles on (a) are mapped to small ellipses on (b) under the T-Map, with the same eccentricity. In (c), we show the histogram of the norm of the BC. It accumulates at 0.21, meaning that the conformality distortion is uniform everywhere. Figure 21 shows the energy $E_2(\mu(f_n)) := \|\mu(f_n)\|_\infty$ in each iterations with different initializations. (a) shows the energy in each iterations with an arbitrary initialization. The algorithm converges in 20 iterations. Again, if a good initialization is chosen as described in Sect. 5.3, the algorithm converges quickly in less than 5 iterations as shown in (b).

Example 13 In Fig. 22, we compute the extremal parameterization of the multiply-connected human faces with three holes. (a) shows a simple user-defined parameter domain. Using our algorithm, an extremal map parameterizing the human face onto the simple parameter domain with least conformality distortion can be obtained. On the simple parameter domain, structured grids can easily obtained as shown in (a). Using the extremal T-Map, we map the structured grid onto the multiply-connected human face as shown in (b). (c) shows the histogram of the BC norm which illustrates that the obtained map is indeed a T-Map. In (d), we map the checkerboard texture on the parameter domain onto the human face using the

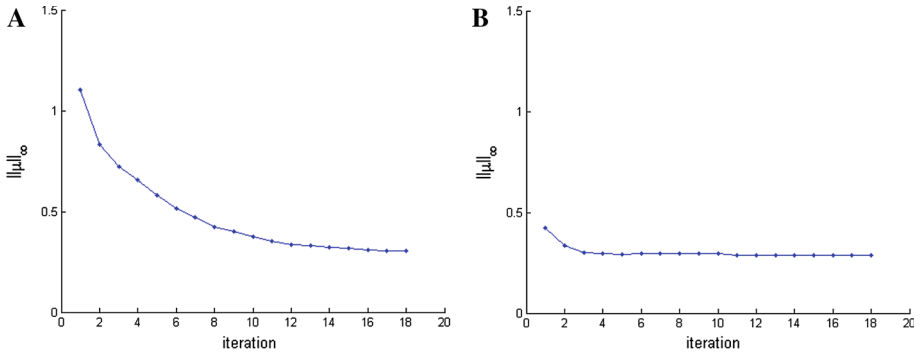


Fig. 21 **a** The energy $E_2(\mu(f_n)) := \|\mu(f_n)\|_\infty$ versus each iterations of Example 10 with an arbitrary initialization. **b** The energy $E_2(\mu(f_n)) := \|\mu(f_n)\|_\infty$ versus each iterations with the initialization proposed in Sect. 5.3

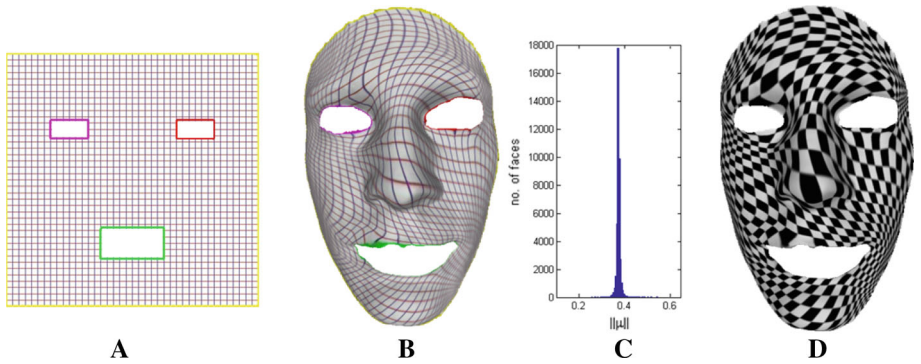


Fig. 22 The extremal parameterization of the multiply-connected human faces with three holes. **a** A simple user-defined parameter domain. On the simple parameter domain, structured grids can easily obtained as shown in (a). In (b), the structured grid is mapped onto the multiply-connected human face using the extremal T-Map. **c** The histogram of the BC norm which illustrates that the obtained map is indeed a T-Map. In (d), the checkerboard texture on the parameter domain is mapped onto the human face using the extremal T-Map

T-Map. This example demonstrates the extremal T-Map can be applied for grid generation on multiply-connected domains or surfaces.

8 Conclusion

In this paper, we present a numerical method to compute the extremal Teichmüller map between arbitrary multiply-connected domains. The domains of interest can either be planar domains or surfaces embedded in \mathbb{R}^3 . Given two multiply-connected domains with boundaries, there exists a unique bijective extremal Teichmüller map(T-Map) between them minimizing the conformality distortion. The T-Map can be considered as the ‘most conformal’ mapping between multiply-connected domains. In this work, we propose an iterative algorithm to obtain the T-Map using the Beltrami holomorphic flow (BHF). The BHF procedure iteratively adjusts the map, based on a sequence of complex-valued functions converging to an optimal Beltrami coefficient associated to the desired extremal T-Map. It produces a sequence of quasi-conformal maps, which converges to the extremal T-Map

minimizing the conformality distortion. We test our proposed algorithms on synthetic 2D multiply-connected domains together with real 3D human faces. Experimental results show that our algorithm computes T-Map between multiply-connected domains accurately and efficiently.

In the future, we will extend our algorithm to compute the extremal Teichmüller map of high-genus surfaces and of surfaces represented by point clouds. Besides, the unique conformality distortion of the extremal T-Map gives us a way to measure the distance between two multiply-connected shapes, namely, the Teichmüller metric. We will explore this research direction to apply the Teichmüller metric for the shape analysis of multiply-connected 2D/3D objects.

Acknowledgments Lok Ming Lui is supported by RGC GRF (Grant No: CUHK401811). Xianfeng Gu is supported in part of NSF Nets 1016286, NSF IIS 0916286, NSF CCF 1081424 and ONR N000140910228.

References

1. Daripa, P.: On a numerical method for quasiconformal grid generation. *J. Comput. Phys.* **96**, 229–236 (1991)
2. Daripa, P.: A fast algorithm to solve nonhomogeneous Cauchy–Riemann equations in the complex plane. *SIAM J. Sci. Stat. Comput.* **13**(6), 1418–1432 (1992)
3. DeLillo, T.K., Kropf, E.H.: Numerical computation of the Schwarz–Christoffel transformation for multiply connected domains. *SIAM J. Sci. Comput.* **33**(3), 3195–3215 (2011)
4. Fischl, B., Sereno, M., Tootell, R., Dale, A.: High-resolution intersubject averaging and a coordinate system for the cortical surface. *Hum. Brain Mapp.* **8**, 272–284 (1999)
5. Fletcher, A., Markovic, V.: *Quasiconformal Maps and Teichmüller Theory*. Oxford graduate text of mathematics, 11 (2007)
6. Gardiner, F., Lakic, N.: *Quasiconformal Teichmüller Theory*. American Mathematics Society (2000)
7. Gu, X.F., Lui, L.M., Yau, S.T.: Convergence of an iterative algorithm for Teichmüller maps via harmonic energy optimization. In: Working Paper (2013)
8. Gu, X., Yau, S.: Computing conformal structures of surfaces. *Commun. Inf. Syst.* **2**(2), 121–146 (2002)
9. Gu, X., Wang, Y., Chan, T.F., Thompson, P.M., Yau, S.-T.: Genus zero surface conformal mapping and its application to brain, surface mapping. *IEEE Trans. Med. Imaging* **23**(8), 949–958 (2004)
10. Haker, S., Angenent, S., Tannenbaum, A., Kikinis, R., Sapiro, G., Halle, M.: Conformal surface parameterization for texture mapping. *IEEE Trans. Vis. Comput. Gr.* **6**, 181–189 (2000)
11. Hale, N., Tee, T.W.: Conformal maps to multiply-slit domains and applications. *SIAM J. Sci. Comput.* **31**(4), 3195–3215 (2009)
12. Hurdal, M.K., Stephenson, K.: Discrete conformal methods for cortical brain flattening. *Neuroimage* **45**, 86–98 (2009)
13. Jin, M., Kim, J., Luo, F., Gu, X.: Discrete surface Ricci flow. *IEEE Trans. Vis. Comput. Gr.* **14**(5), 1030–1043 (2008)
14. Lehto, O., Virtanen, K.: *Quasiconformal Mappings in the Plane*. Springer, New York (1973)
15. Lévy, B., Petitjean, S., Ray, N., Maillot, J.: Least squares conformal maps for automatic texture atlas generation. In: *ACM SIGGRAPH Conference Proceedings* (2002)
16. Lui, L.M., Gu, X.F., Yau, S.T.: Convergence of an iterative algorithm for Teichmüller maps via generalized harmonic maps. arXiv: 1307.2679v1 (<http://arxiv.org/abs/1307.2679>) (2013)
17. Lui, L.M., Lam, K.C., Wong, T.W., Gu X.F.: Texture map and video compression using Beltrami representation. *SIAM J. Imaging Sci.* **6**(4), 1880–1902 (2013)
18. Lui, L.M., Lam, K.C., Yau, S.T., Gu, X.F.: Teichmüller extremal mapping and its applications to landmark matching registration. arXiv:1211.2569 (<http://arxiv.org/abs/1210.8025>)
19. Lui, L.M., Wong, T.W., Gu, X.F., Chan, T.F., Yau, S.T.: Compression of surface diffeomorphism using Beltrami coefficient. *IEEE Comput. Vis. Pattern Recognit. (CVPR)*, pp. 2839–2846 (2010)
20. Lui, L.M., Wong, T.W., Gu, X.F., Thompson, P.M., Chan, T.F., Yau, S.T.: Hippocampal shape registration using Beltrami holomorphic flow. *Med. Image Comput. Comput. Assist. Interv. (MICCAI), Part II, LNCS* **6362**, 323–330 (2010)
21. Lui, L.M., Wong, T.W., Zeng, W., Gu, X.F., Thompson, P.M., Chan, T.F., Yau, S.T.: Optimization of surface registrations using Beltrami holomorphic flow. *J. Sci. Comput.* **50**(3), 557–585 (2012)

22. Mastin, C.W., Thompson, J.F.: Discrete quasiconformal mappings. *Zeitschrift für angewandte Mathematik und Physik (ZAMP)* **29**(1), 1–11 (1978)
23. Mastin, C.W., Thompson, J.F.: Quasiconformal mappings and grid generation. *SIAM J. Sci. Stat. Comput.* **5**(2), 305–310 (1984)
24. Porter, R.M.: An interpolating polynomial method for numerical conformal mapping. *SIAM J. Sci. Comput.* **23**(3), 1027–1041 (2001)
25. Reich, E.: Extremal Quasi-conformal Mappings of the Disk. *Handbook of Complex Analysis: Geometric Function Theory*, vol 1, Chapter 3. pp. 75–135 (2002)
26. Strebel, K.: On quasiconformal mappings of open riemann surfaces. *Comment. Math. Helvetici* **53**, 301–321 (1978)
27. Wang, Y., Lui, L.M., Gu, X., Hayashi, K.M., Chan, T.F., Toga, A.W., Thompson, P.M., Yau, S.-T.: Brain surface conformal parameterization using riemann surface structure. *IEEE Trans. Med. Imaging* **26**(6), 853–865 (2007)
28. Weber, O., Myles, A., Zorin, D.: Computing extremal quasiconformal maps. *Comput. Gr. Forum* **31**(5), 1679–1689 (2012)
29. Wong, T.W., Zhao, H.: Computation of quasiconformal surface maps using discrete Beltrami flow. *UCLA CAM report* 12–85 (2013)
30. Yang, Y.L., Kim, J., Luo, F., Hu, S., Gu, X.F.: Optimal surface parameterization using inverse curvature map. *IEEE Trans. Vis. Comput. Gr.* **14**(5), 1054–1066 (2008)
31. Zeng, W., Gu, X.: Registration for 3D surfaces with large deformations using quasi-conformal curvature flow. In: *IEEE Conference on Computer Vision and Pattern Recognition (CVPR11)*, Jun 20–25, : Colorado Springs, Colorado, USA (2011)
32. Zeng, W., Lui, L.M., Shi, L., Wang, D., Chu, W.C., Cheng, J.C., Hua, J., Yau, S.T., Gu, X.F.: Shape analysis of vestibular systems in adolescent idiopathic scoliosis using geodesic spectra. *Med. Image Comput. Comput. Assist. Interv.* **13**(3), 538–546 (2010)
33. Zeng, W., Lui, L.M., Luo, F., Chan, T.F., Yau, S.T., Gu, X.F.: Computing quasiconformal maps using an auxiliary metric and discrete curvature flow. *Numer. Math.* **121**(4), 671–703 (2012)